Journal of Volcanology and Geothermal Research 427 (2022) 107558

Contents lists available at ScienceDirect

Journal of Volcanology and Geothermal Research

journal homepage: www.journals.elsevier.com/journal-of-volcanology-and-geothermal-research

The complexities of assessing volcanic hazards along the Cameroon Volcanic Line using spatial distribution of monogenetic volcanoes

Christoph Schmidt [a,*], Christian Laag [b], Melody Whitehead [c], Jörn Profe [d], Festus Tongwa Aka [e], Takeshi Hasegawa [f], Gabor Kereszturi [c]

[a] Institute of Earth Surface Dynamics, University of Lausanne, Quartier UNIL-Mouline, Géopolis, 1015 Lausanne, Switzerland
[b] Université Paris Cité, Institut de physique du globe de Paris, CNRS, F-75005 Paris, France
[c] Volcanic Risk Solutions, School of Agriculture and Environment, Massey University, Private Bag, 11 222 Palmerston North, New Zealand
[d] Department of Geography, Geoinformatics and Remote Sensing, Justus-Liebig-University Gießen, Senckenbergstraße 1, 35390 Gießen, Germany
[e] Department of Physical Sciences, School of Mathematics and Science, CCBC, Essex Campus, 7201, Rossville Boulevard, Baltimore, MD 21237, USA
[f] Department of Earth Sciences, College of Science, Ibaraki University, 2-1-1 Bunkyo, Mito 310-8512, Japan

ARTICLE INFO

Keywords:
Scoria cone
Maar
Morphometry
Point pattern
Volcanic hazards
Basalt

ABSTRACT

Volcanic eruptions represent hazards for local communities and infrastructure. Monogenetic volcanoes (usually) erupt only once, and then volcanic activity moves to another location, making quantitative assessment of eruptive hazards challenging. Spatio-temporal patterns in the occurrence of these eruptions may provide valuable information on locations more likely to host future eruptions within monogenetic volcanic fields. While the eruption histories of many stratovolcanoes along the Cameroon Volcanic Line (CVL) are relatively well studied, only fragmentary data exist on the distribution and timing of this region's extensive monogenetic volcanism (scoria cones, tuff rings, maars). Here, we present for the first time a catalog of monogenetic vents on the CVL. These were identified by their characteristic morphologies using field knowledge, the global SRTM Digital Elevation Model (30 m resolution), and satellite imagery. More than ~1100 scoria cones and 50 maars/tuff rings were identified and divided into eight monogenetic volcanic fields based on the visual assessment of clustering and geological information. Spatial analyses show a large range of areal densities between the volcanic fields from >0.2 km^{-2} to 0.02 km^{-2} from the southwest towards the northeast. This finding is in general agreement with previous observations, indicating closely spaced and smaller edifices typical of fissure-fed eruptions on the flanks of Bioko and Mt. Cameroon in the southwest, and a more focused plumbing system resulting in larger edifices of lower spatial density towards the northeast. Spatial patterns were smoothed via kernel density estimates (KDE) using the Summed Asymptotic Mean Squared Error (SAMSE) bandwidth estimator, the results of which may provide an uncertainty range for a first-order hazard assessment of vent opening probability along the CVL. Due to the scarce chronological data and the complex structural controls across the region, it was not possible to estimate the number of vents formed during the same eruptive events. Similarly, the percentage of hidden (buried, eroded) vents could not be assessed with any acceptable statistical certainty. Furthermore, the impact of different approaches (convex hull, minimum area rectangle and ellipse, KDE isopaches) to define volcanic field boundaries on the spatial distribution of vents was tested. While the KDE boundary definition appears to reflect the structure of a monogenetic volcanic field better than other approaches, no ideal boundary definition was found. Finally, the dimension of scoria cones (approximated by their basal diameters) across the CVL was contrasted to the specific geodynamic setting. This region presents a complex problem for volcanic hazard analysis that cannot be solved through basic statistical methods and, thus, provides a potential testbed for novel, multi-disciplinary approaches.

* Corresponding author.
E-mail address: christoph.schmidt@unil.ch (C. Schmidt).

https://doi.org/10.1016/j.jvolgeores.2022.107558
Received 5 November 2021; Received in revised form 7 April 2022; Accepted 16 April 2022
Available online 22 April 2022

1. Introduction

Monogenetic eruptions usually occur over short timescales (days to years) and in new locations within a volcanic field. These eruptions pose significant hazards to communities living close-by and expose life-line infrastructure through deposition of tephra, lava flows or pyroclastic density currents (e.g., Ort et al., 2008; Connor et al., 2012; Del Negro et al., 2013; Wilson et al., 2014; Bebbington, 2015; Kereszturi et al., 2017). Monogenetic eruptions can further cause secondary hazards related to extensive outgassing, landscape modification, landslides, and/or surface/groundwater contamination (e.g., Watts and Waythomas, 2003; Manville, 2010; Aka and Yokoyama, 2012; Issa et al., 2014; Valente et al., 2022). A vivid demonstration of secondary volcanic hazards is the 1986 CO_2 outburst from Lake Nyos, a maar located on the Cameroon Volcanic Line (CVL), with lethal effects for more than 1500 people (Freeth and Kay, 1987; Kling et al., 1987).

We here adopt the definition of 'monogenetic volcanoes' from Németh and Kereszturi (2015), as a volcano created by one or more small eruptions with a maximum of 1 km^3 of erupted material and an eruption duration of ≤100 years. While the activity phase of a single monogenetic volcano is short, monogenetic volcanic fields – usually comprising in the order of 10^2–10^3 individual centers – commonly evolve over timescales of 10^6–10^7 years, equaling or exceeding the typical lifetime of a composite (polygenetic) volcano (Condit and Connor, 1996; Guilbaud et al., 2012; Kereszturi et al., 2013; Grosse et al., 2020). Monogenetic volcanoes may occur in areas spanning 100–1000's km^2 (e.g., Le Corvec et al., 2013). Due to the dispersed magmatic plumbing system of monogenetic volcanoes, spatio-temporal hazard estimation and the prediction of next vent locations are challenging (e.g., Bebbington, 2013). Therefore, point location and time-series analyses

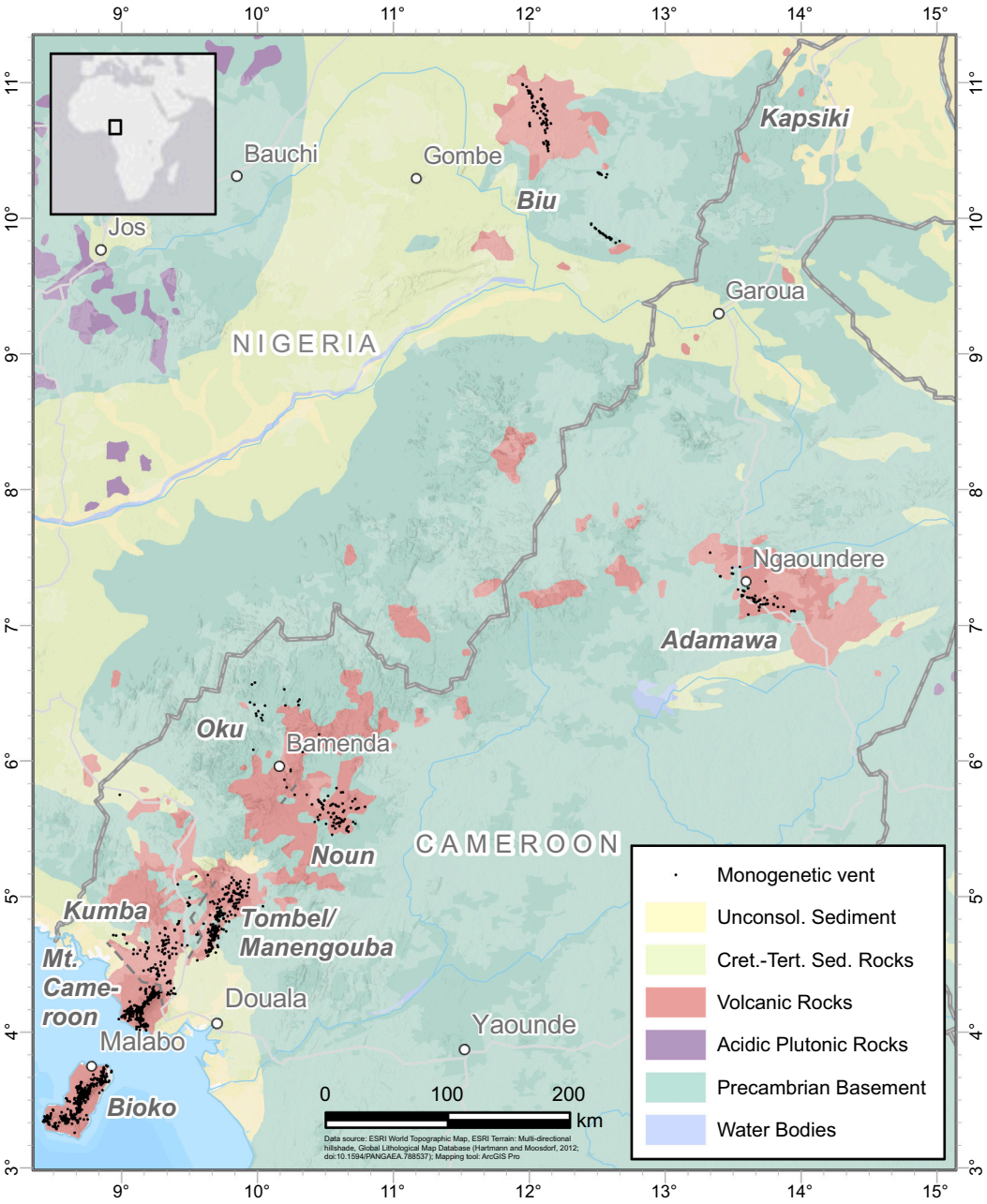

Fig. 1. Geology and overview of monogenetic volcanic fields and digitized monogenetic volcanoes along the Cameroon Volcanic Line as relevant to this study. Names of monogenetic volcanic fields are indicated in bold and italics. Information on main tectonic faults along the CVL can be found, e.g., in Moreau et al. (1987), Marcel et al. (2018) and Njeudjang et al. (2020).

are often used to estimate the likelihood of future eruptions (e.g., Marzocchi and Bebbington, 2012; Valentine and Connor, 2015; Nieto-Torres and Martin Del Pozzo, 2019).

The CVL in Central Africa comprises eight monogenetic volcanic fields with an estimated total area of ~17,000 km^2, with individual fields in the order of ~700 km^2 to ~4000 km^2 (Fig. 1). The CVL is situated in a unique tectonic environment at the transition from oceanic to continental crust, and therefore represents a natural laboratory for assessing the geochemical evolution of alkaline magmas with various degrees of crustal contamination and mixing (e.g., Kamgang et al., 2008, 2010; Asaah et al., 2015). Composite volcanoes on the CVL have received great attention and are generally well-characterized for their petrography, geochemistry and geochronology (e.g., Fitton and Dunlop, 1985; Marzoli et al., 1999; Aka et al., 2004, 2018; Yokoyama et al., 2007; Njome et al., 2008; Kamgang et al., 2008, 2010; Kagou Dongmo et al., 2010; Pouclet et al., 2014; Asaah et al., 2015). However, the composite volcanoes are outnumbered by a large population of monogenetic volcanoes, including scoria cones, tuff rings, maar-diatremes and associated lava flows, which have received much less attention so far, thus representing a generally overlooked volcanic hazard in Central Africa (see also Brown et al., 2015). This is illustrated by the fact that ~46% of the total population of Cameroon (~9 Mio. people) lives <100 km away from a volcano (both polygenetic and monogenetic) showing activity during the Holocene, and five out of the country's ten largest cities including critical infrastructure (airports, harbors) are within this zone (Brown et al., 2015).

This study presents the first catalog of the spatial distribution of monogenetic volcanoes for the CVL constructed using the analysis of aerial imagery and a Digital Elevation Model (DEM), supplemented by new field observations. The obtained spatial data (i.e., vent locations) are analyzed statistically for their areal density and distribution using clustering analyses and Kernel Density Estimation (KDE) techniques. The catalog compiled here may constitute a first step towards developing a multi-country baseline dataset in this region and may provide valuable information for the assessment of volcanic hazards associated with these unique and complex monogenetic volcanic fields.

2. Geological setting

The CVL is a ~1700 km long and ~N30°E to ~N45°E trending tectono-magmatic province, stretching from the oceanic islands of Annobón, Sao Tomé, Príncipe and Bioko to Mt. Oku on the continental sector, where the lineament splits into three branches continuing to the Biu plateau (Nigeria), the Kapsiki plateau and the Adamawa plateau (Fig. 1). It crosses the ocean-continent boundary close to Mt. Cameroon. While different definitions of the CVL exist, we follow the one proposed by Njome and de Wit (2014) and include the Kapsiki plateau. In addition to the oceanic volcanic islands, the CVL encompasses the four polygenetic volcanic centers of Mt. Cameroon (with Etinde), Mt. Manengouba, Mt. Bambouto and Mt. Oku as well as the basaltic plateaus of Biu, Adamawa and Kapsiki. The Kapsiki area, however, was not further considered for vent analyses as there is no evidence of Neogene volcanic activity (Njome and de Wit, 2014). In between the polygenetic centers, graben structures partly filled with basaltic lava flows host monogenetic volcanic structures, including scoria cones, tuff rings and maar volcanoes (e.g., Fitton, 1987; Njome et al., 2008; Pouclet et al., 2014). A large number of scoria cones can also be found at the flanks of the central volcanoes (e.g., Mt. Cameroon, Mt. Manengouba).

Magmatic activity along the CVL started in the late Cretaceous, or early Paleogene, with the emplacement of plutonic bodies in the central and northern parts (Jacquemin et al., 1982; Fitton, 1987 and references therein). The oldest volcanic rocks dated at 51.8 ± 1.2 Ma (Moundi et al., 2007) were found at Foumban, Mt. Bambouto. A large number of K/Ar and a few more recent Ar/Ar ages of extrusive rocks suggest that there is no age progression along the CVL (e.g., Fitton and Dunlop, 1985; Marzoli et al., 1999, 2000; Montigny et al., 2004; Aka et al., 2018). While plutonic activity appears to have ceased after ~30 Ma north of Mt. Oku, eruptions are documented throughout the Neogene and Quaternary southwest of Mt. Oku (see compilation of chronometric data in Njome and de Wit, 2014; Aka et al., 2018). The only presently active polygenetic volcano is Mt. Cameroon with a total of seven confirmed eruptions in the last century and an unconfirmed, short-lived eruption in 2012 (Suh et al., 2003; Njome et al., 2008).

Table 1 summarizes relevant available chronometric data for mainly monogenetic volcanic activity along the CVL. All monogenetic fields show Pleistocene activity and few of them witnessed eruptions in the Holocene (Bioko, Mt. Cameroon and probably Oku and Tombel/Manengouba). Given the fragmentary age data on monogenetic eruptions, it is difficult to recognize spatio-temporal patterns of activity. More context information aiding the interpretation of these numeric ages is provided in the Supplementary Materials; an extensive review of age data is presented by Aka et al. (2018; their Table S2).

Although there is no unified geodynamic model, it has been proposed that the magmatic activity along the CVL is linked to an intraplate extensional stress regime and thinning of the lithosphere with deep mantle upwelling and pressure release inducing the volcanism (e.g., Maluski et al., 1995; Burke, 2001). In general, previously existing tectonic structures such as Neoproterozoic shear zones and faults are assumed to play a role for the distribution of volcanism along the CVL (e.g., Fitton, 1987; Déruelle et al., 1991). For instance, Moreau et al. (1987) argue that four major lineament directions (N-S, N70°E, N45°W, E–W) control magma ascend along the CVL. In particular the western branch of the Central African Shear Zone (including the Adamawa Shear Zone; ~N60°E–N70°E) is believed to at least partly determine the emplacement of magmatic and volcanic complexes (see summary in Déruelle et al., 1991, Njome and de Wit, 2014; and recent review in Adams, 2022). A detailed understanding of the origin of the volcanic activity is further limited by the scanty and scattered radiometric age data for the entire CVL (see Table 1 and Aka et al., 2018). Tectonic, petrographic and geochemical aspects of the CVL are covered in reviews and regional studies by, e.g., Sato et al. (1990), Déruelle et al. (1991, 2007), Tamen et al. (2007), Nkouathio et al. (2008), Njome and de Wit (2014), Asaah et al. (2015), Yamgouot et al. (2016), Ngwa et al. (2017), Tiabou et al. (2019) and Temdjim et al. (2020).

3. Methods

3.1. Mapping monogenetic volcanoes

Monogenetic volcanoes represent the surface expression of point-like mantle-sourced magmas (Valentine et al., 2017; Smith and Cronin, 2021), while they can also form multiple vents on the surface (Dóniz-Páez, 2015; Graettinger, 2018). We here specifically also consider parasitic cones on the flanks of polygenetic vents as monogenetic volcanoes. Digitizing individual craters can result in an overestimation of vent density from a volcanic hazards perspective as multiple vents may represent a single eruptive episode (e.g., Guilbaud et al., 2009; Runge et al., 2014). On the other hand, an underestimation of eruptive events may occur if multiple events created a composite vent that is misinterpreted to derive from a single eruption. Monogenetic volcanoes were digitized manually, with a point-feature representing the location of the approximate center of each recognized scoria cone or maar. In case of overlapping cone or maar structures, we recorded them as individual features if two distinct vents could be distinguished. This was achieved using a combination of existing geological maps (1:200,000; published by S.G.A.E.F. Cameroon), field information, satellite imagery (mainly Landsat and Sentinel 2 with 30 m and 10 m resolution, respectively) and a multi-directional hillshade (ArcGIS Pro) derived from a Shuttle Radar Topography Mission (SRTM) Digital Elevation Model (DEM) with 30 m resolution, using the WGS84 UTM32N projection.

The general morphology was used to identify and classify volcanic

Table 1
Published chronometric data for monogenetic volcanic activity along the Cameroon Volcanic Line. More context information on dating methods and stratigraphy is provided in the Supplementary Materials.

Volcanic field	Name / Location	Dated feature	Method	Age [ka]	Reference
Sao Tomé	Various locations	Six scoria cones	$^{40}Ar/^{39}Ar$	860–36	Barfod and Fitton (2014)
Bioko	Various locations	Lava flow	Paleomagnetism	<780	Piper and Richardson (1972)
	Various locations	Scoria cones	Historical records	<0.2	Piper and Richardson (1972)
Mt. Cameroon	Various locations	Scoria cones	Historical records	> 0.02	Ateba et al. (2009)
Kumba	Barombi Mbo maar	Lava flow	K/Ar	<1050 ± 70	Cornen et al. (1992)
	Barombi Mbo maar	Total carbon from drill core	^{14}C	>22 BP	Maley et al. (1990); Cornen et al. (1992)
	Barombi Mbo maar		K/Ar	240 ± 20	Aka (2000)
	Barombi Mbo maar		K/Ar	200 ± 20	Aka (2000)
	Barombi Mbo maar	Basaltic lava	K/Ar (whole-rock)	510, 200, 80	Chako Tchamabé et al. (2014)
	Barombi Koto maar	Basaltic lava	K/Ar	50 ± 20	Chako Tchamabé et al. (2014)
Tombel/ Manengouba	Njombé	Basaltic lava	K/Ar	10 ± 120	Nkouathio et al. (2008)
	Nlohé	Hawaiite lava	K/Ar	120 ± 120	Nkouathio et al. (2008)
	Various locations	Lava flows	$^{40}Ar/^{39}Ar$	240–50	Lee (1994), as cited in Kagou Dongmo et al. (2001)
Noun	Yupé (Bamendjing)	Scoria cone	K/Ar	4590 ± 120	Wotchoko et al. (2005); Wandji et al. (2010)
	Kamkop (Baleng)	Basaltic lava flow	K/Ar	4150 ± 110	Wandji et al. (2010)
	Galim (Mbéhuè)	Scoria cone	K/Ar	2040 ± 200	Wandji et al. (2010)
	Boya	Scoria cone	K/Ar	1700 ± 190	Wandji et al. (2010)
	Tchanda Bororo (Baleng)	Scoria cone	K/Ar	400 ± 100	Wandji et al. (2010)
	Bamoun (south of Noun plain)	Basanitic lava flow	K/Ar	820 ± 50	Moundi et al. (2007)
	Totap (NE of Mt. Bambouto and W of the Noun plain)	Basanitic scoria cone	K/Ar	480 ± 15	Kagou Dongmo et al. (2010)
Adamawa	Various locations	Basaltic lava flows	K/Ar	910 ± 60	Temdjim et al. (2004)
Oku	Nyos maar	Basalt	K/Ar	>350	Freeth and Rex (2000)
	Nyos maar	Carbonized wood	^{14}C	0.4	Lockwood and Rubin (1989)
	Nyos maar	Basalt	U-series	10–5	Aka et al. (2008)
	Nyos maar	Bedrock quartz	Thermoluminescence	<12.3 ± 1.5	Schmidt et al. (2017a)
	Nyos maar		Stratigraphy in relation to Njupi	>3.4 BP	Zogning et al. (1997)
	Lake Njupi	Bulk carbon	^{14}C	>3.4 BP	Zogning et al. (1997)
	South of Lake Oku	Basaltic lava flow	K/Ar	890 ± 100	Konfor et al. (2007)
Biu	Northern end of Biu plateau	Basalt / basanite	K/Ar	<840 ± 90	Fitton and Dunlop (1985)
	Various locations	Basalt	K/Ar	<5000–1400	Baudin (1991), as cited in Lar et al. (2013)
	Lake Tilla	Organic matter	^{14}C	>11.1 BP	Salzmann (2000)

landforms (Kervyn et al., 2012; Seib et al., 2012; Dóniz-Páez, 2015; Pedrazzi et al., 2020). A positive relief with distinct circular, breached or horseshoe-shaped central crater, a basal width of a few hundred meters and a height of ~50–300 m were considered typical for a scoria cone (without distinguishing simple, multiple, complex and breached scoria cones). A more or less circular depression below the surrounding surface and occupied by a lake or a leveled sedimentary filling bordered by the flanks of a tephra ring were interpreted as phreatomagmatic volcanoes, including maars and tuff rings. The flanks of the latter are generally less steep and lower than those of scoria cones. No further discrimination was applied to distinguish between maars and tuff rings due to the coarse DEM resolution. More information on the general morphology of monogenetic volcanoes in relation to their genesis is given in the Supplementary Materials. The results have, to a limited extent, been verified through a field visit within the Noun and Tombel volcanic fields (Fig. 2). Identified scoria cones were validated against two previously published maps for Bioko (Piper and Richardson, 1972) and the Tombel graben (Nkono et al., 2009). In case of mismatch, missing scoria cones were added to our data set to compile a catalog as complete as possible.

Annobón, Sao Tomé and Principé islands were excluded from spatial and statistical analyses, because they do not provide a sufficient number of unambiguously identifiable monogenetic vents that would allow for robust hazard assessment.

3.2. Volcanic field boundary definition

Individual vents were assigned to eight monogenetic volcanic fields based on geological and tectonic information and the visual assessment of large-scale vent distribution. The definition of the boundary of a particular volcanic field can have far-reaching consequences on the outcome of vent distribution analyses and hence on hazard assessment (see Runge et al., 2015 for a detailed discussion). To evaluate the impact of different boundary definitions on the outcome of point-pattern analyses (see Section 3.4), we tested four of those definitions for the Bioko, Noun and Biu volcanic fields on the CVL: (1) convex hull, (2) minimum area rectangle, (3) minimum area ellipse, and (4) probability contours resulting from Kernel Density Estimation (KDE); see Supplementary Materials for technical details. To facilitate comparability with previously obtained datasets on vent distribution (e.g., Le Corvec et al., 2013; Haag et al., 2019; Cañón-Tapia, 2021), we chose the convex hull boundary definition as the standard approach for the eight monogenetic fields on the CVL. However, we do not adopt the assumption that a single volcanic field boundary method represents the optimum structure for all of these monogenetic volcanic fields, nor that this convex hull most accurately represents the subsurface plumbing or complete surface locations at which future eruptions may occur.

3.3. Grouping vents into events

The mapped vents can be grouped into eruptive events in locations where this behavior is observed, e.g., for a series of aligned scoria cones that formed during the last eruption of Mt. Cameroon. This is an important step for monogenetic volcanic fields exhibiting multiple vent eruptions as the temporal recurrence rate is often estimated by comparing the number of eruptions with the overall time-period during which a volcanic field has been active. Runge et al. (2014) developed a

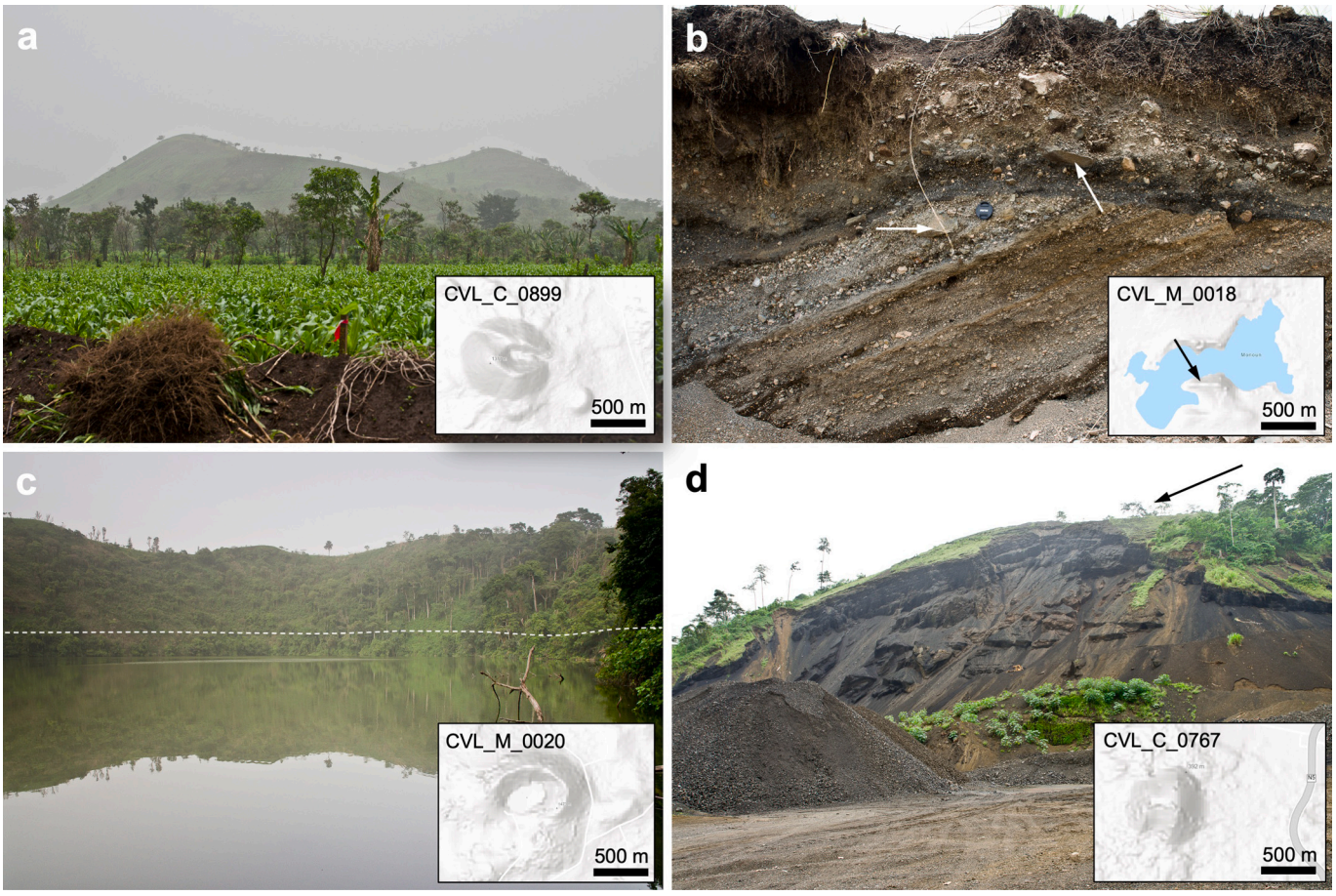

Fig. 2. Field photographs of some monogenetic features along the Cameroon Volcanic Line, together with their equivalent SRTM multi-directional hillshades shown in the inset. (a) A Quaternary, pristine scoria cone in the Noun volcanic field ~5 km northwest of Foumbot (view to northwest). (b) Poorly to moderately sorted pyroclastic deposits exposed within a tephra ring succession at the south of Lake Monoun (view to west). The white arrows show excavated lithics from the Precambrian basement (orthogneiss). The black arrow in the inset marks the position of the shown outcrop. (c) Crater lake accumulated within the Baleng maar in the Noun volcanic field, ~8 km north of Bafoussam. The estimated level of the pre-eruptive basement is indicated by the dashed line (view to northeast). (d) Exposed succession of a scoria cone close to Penja in the Tombel/Manengouba volcanic field, showing non-oxidized scoria with coarse to fine lapilli grain size. The crater location is indicated by the black arrow (view to southwest). The identifiers given for each vent shown here are indicated in the inset.

'vents-to-events' routine for volcanic fields in Saudi Arabia based on estimated distributions of event length, width and deviation from dominant stress-field and fault orientation. This method collapses these multiple vent eruptions into their most likely eruption events. However, for this method to work consistently across a region, the distribution of these properties is assumed constant in space and time and consequently, a single dominant stress direction must be determined for each volcanic field. The probability of a vent belonging to one event is then higher where an event is aligned more closely to this principal direction. Accounting for multiple stress directions is possible but significantly increases the problem of overfitting (i.e., by increasing the number of fitting parameters without increasing the variance within the distribution or the number of points to be fitted).

In Runge et al. (2014), three distinct priors (based on analog fields, expert judgement, and a set of non-informative values) were updated to posterior distributions tailored specifically for the field of interest (in their case Harrat Rahat) using historical events. The strong tectonic controls on the vent distribution and the presence of rifting (e.g., Tombel Graben) makes the chosen approach appropriate for assessing the potential grouping of the digitized vents into volcanic events.

The 'vents-to-events' code was rewritten in **R** (R Core Team, 2021) for the explicit application to the CVL during this work, and the main stress directions of all eight monogenetic fields on the CVL were estimated from previous publications and cross-checked against the main orientation of fault lines on the SRTM DEM (see Fig. S8). These estimates were further compared to the results from a SAMSE (Summed Asymptotic Mean Squared Error) kernel bandwidth estimator (see Section 3.5).

3.4. Spatial organization using point pattern analysis

The spatial distribution of volcanic vents may reveal important underlying geological and volcanic information, including magma source patterns in the mantle together with crustal tectonic structures (e.g., Le Corvec et al., 2013; Cañón-Tapia, 2021). To assess the likelihood that any patterns within each of these volcanic fields were obtained from a non-random distribution, we applied first- and second-order randomness test statistics (Clark-Evans and Ripley's K) which compare properties of the observed points to the null hypothesis of complete spatial randomness (as described by a homogeneous Poisson Process). The Clark-Evans first-order test compares distances between observed vents with the distances expected between randomly placed vents (Clark and Evans, 1954). The Ripley's $K(r)$ second-order test compares the number of vents within a distance d of each vent to the expected number of vents for a random distribution (Ripley, 1979). Instead of $K(r)$, $L - r$ was plotted, with $L = (K(r)/\pi)^{0.5}$, because $L - r$ is zero for randomly distributed points, enabling an easier visual assessment of the distribution pattern. For details on calculations and code, see the Supplementary Materials.

Table 2
Summary of results of the statistical nearest neighbor analyses of each monogenetic volcanic field (expected mean nearest neighbor distance $r_e = (2 \cdot \mathrm{sqrt}(N/A))^{-1}$; $R = r_0/r_e$, where $r_0 = \frac{\sum r}{N}$ is the observed mean nearest neighbor distance with $\sum r$ being the summation of nearest neighbor distances).

Name	Bioko	Mt. Cameroon	Kumba	Tombel/Manengouba	Noun	Oku	Adamawa	Biu
Total number *N* of identified vents	314	288	109	194	69	25	56	101
Scoria cones	313	286	104	190	60	11	42	100
Maars	1	2	5	4	9	14	14	1
Area *A* of convex hull [km^2]	1.35E+03	7.31E+02	3.90E+03	1.84E+03	1.32E+03	3.04E+03	1.39E+03	3.48E+03
Areal density *N/A* [km^{-2}]	2.24E-01	3.81E-01	2.59E-02	1.02E-01	4.62E-02	5.60E-03	3.61E-02	2.59E-02
Mean distance [km]	0.834	0.574	1.847	1.208	1.968	3.188	1.306	1.232
Standard deviation 1σ [km]	0.610	0.467	1.434	0.800	1.646	2.923	1.178	1.307
Standard deviation 2σ [km]	1.221	0.935	2.869	1.600	3.293	5.846	2.355	2.614
Minimum distance [km]	0.051	0.111	0.111	0.157	0.313	0.031	0.111	0.156
Maximum distance [km]	4.107	4.332	7.451	4.385	9.005	10.790	4.644	9.233
Skewness	2.58	2.96	1.50	1.16	2.13	1.61	1.41	3.21
Kurtosis	8.85	16.35	3.09	1.10	5.19	2.17	1.32	15.28
r_e [km]	1.056	0.810	3.108	1.568	2.327	6.682	2.632	3.108
R	0.77	0.67	0.61	0.75	0.85	0.47	0.51	0.38
p-value	0.002	0.002	0.002	0.002	0.028	0.002	0.002	0.002
Implication	Clustered	Clustered	Clustered	Clustered	Clustered	Clustered	Clustered	Clustered

3.5. Spatial hazard assessment using Kernel Density Estimates (KDE)

Due to the scarcity of age data for monogenetic volcanoes on the CVL (e.g., Aka et al., 2018), we restrict the hazard assessment to the spatial dimension, utilizing the catalog of vents compiled in this paper. Kernel Density Estimates (KDE) can be used to estimate the underlying distribution from which the observed vents have occurred. Essentially, 2D kernels are placed on all known vent locations, and a surface is constructed through the summing of these kernels across the area. The actual surface estimates are a function of vent location, kernel shape, and kernel bandwidth, and as such, these properties may have a significant effect on the resulting estimate. If it is assumed that the distribution of past, observed vents is governed by the same magmatic and tectonic influences as relevant for the location of future vents, they can be used as an estimate for future vent locations in probabilistic forecasting models (e.g., Lutz and Gutmann, 1995; Connor and Connor, 2009; Bebbington, 2013; Connor et al., 2019).

KDEs may also be used for volcanic field boundary definition (see Section 3.2), as they provide a way of smoothing these vent locations into a more organic field shape. Results of KDE calculations are presented here as contour maps, visualizing either spatial vent density percentiles or absolute spatial vent density (number of vents per m^2).

3.6. Scoria cone dimensions

The scoria cone geometry and morphology can be indicative of syn-eruptive factors, such as magma geochemistry, tectonic environment and eruption styles (e.g., Settle, 1979; Fornaciai et al., 2012; Kereszturi et al., 2012), and subsequent erosional processes (Wood, 1980; Dóniz et al., 2011; Kereszturi and Németh, 2016). In particular, basal width (W_{co}) can change as a function of the erupted lava volume (Kervyn et al., 2012), and is thus a good overall size indicator parameter. In this study, the longest diameter, W_{max}, and the shortest diameter, W_{min}, were measured from the SRTM DEM and its derivatives (e.g., hillshade). The basal width was calculated as an arithmetic mean of W_{max} and W_{min}. Scoria cones with advanced erosion were discarded from this analysis. Besides basal width, cone eccentricity *e* was calculated as

$$e = \sqrt{1 - \frac{\left(\frac{W_{min}}{2}\right)^2}{\left(\frac{W_{max}}{2}\right)^2}}.$$

4. Results

4.1. Catalog of monogenetic volcanoes

In total, we identified 1106 scoria cones and 50 maars/tuff rings on the CVL. The data is available as a xlsx-file as Supplementary Data with the intention to be updated by future studies (scoria cones are indicated by names "CVL_C_…", while maars/tuff rings carry names "CVL_M_…"). A summary of the statistics for each volcanic field is given in Table 2.

The catalog was tested for completeness and accuracy using published vent location maps. Comparing the vent map for Bioko by Piper and Richardson (1972) created through field work with our catalog reveals some georeferencing inaccuracies, causing lateral offset of obviously identical vents. Ignoring these offsets, we missed ~78 vents registered by Piper and Richardson (1972), corresponding to an accuracy of ~75%. The inspection of the overlooked vents reveals that the great majority are invisible on the DEM, and that those vents can probably only be identified with higher resolution data combined with field work. The missed vents and a further ~50 newly identified vents were also added to the location database.

The Tombel graben was also chosen to compare our vent catalog with the map created by Nkono et al. (2009) using SRTM DEM data and Landsat satellite imagery. An overlay of both datasets for a subarea of the Tombel/Manengouba volcanic field is shown in Fig. S4 and confirms that we have captured all but two vents registered by Nkono et al. (2009), giving an accuracy of 99%. In addition, we could identify another ~70 vents previously not seen.

While we took great care to not include false positives (i.e., non-volcanic landforms, such as inselbergs, resembling a scoria cone), we cannot rule out that the compiled dataset contains a small number of erroneously mapped features. However, pending possibilities for further ground-truthing, we were not able to quantify the potential bias introduced by false positives. A detailed description of each monogenetic volcanic field regarding the mapped vents and their spatial characteristics is provided in the Supplementary Materials.

4.2. Grouping vents into events

Table 3 summarizes the main strike directions of all volcanic fields, as determined independently from previous publications, existing

Table 3
Main strike directions as previously published, extracted from geologic maps and DEMs, and as resulting from kernel-based boundary definitions (bandwidth matrix). The last column gives the distribution pattern obtained for Ripley's $K(r)$ function when the convex hull boundary definition is chosen. Anisotropic bandwidths from calculating KDEs (SAMSE) are shown in the second-to-last column.

Volcanic field	Published strike direction	Reference	Strike direction from maps and DEMs	Strike direction from bandwidth matrix	Anisotropic bandwidths from KDEs	Distribution pattern from $K(r)$
Bioko	N30°E	Marcel et al., 2018	N40°E	N42°E	3087 m; 2913 m	Clustering ≳≈ 350 m
Mt. Cameroon	N40–50°E	Ateba et al., 2009	N40–50°E	N39°E	1754 m; 1583 m	Clustering ≳≈ 100 m
Kumba	N60°W	Nkono et al., 2009	N50°W (northern part)	N17°E	4489 m; 3156 m	Clustering >0 m
	N10°W	Marcel et al., 2018	N40°E (southern part)			
Tombel/Manengouba	N40°E	Nkono et al., 2009	N40°E	N21°E	2338 m; 3091 m	Clustering ≳≈ 500 m
	N30°E, N50°W, N60°E	Pouclet et al., 2014				
Noun	N45°E, N85°E	Marcel et al., 2018	N60°E, N15°E	N62°W	4814 m; 2593 m	Clustering ≳≈ 1200 m
Oku	N0°E, N25°W	Konfor et al., 2007	N50°W, N10°W, N40°E, N60°E, N15°E	N20°W	6650 m; 5089 m	Clustering ≳≈ 2000 m
	N30–45°E	Marcel et al., 2018				
Adamawa	N70°E	Déruelle et al., 2007	N60°E, N40°W (?)	N60°W	5808 m; 4126 m	Clustering >0 m
	N30–80°E	Njeudjang et al., 2020				
	N30–70°E	Awé et al., 2021				
Biu	–	–	N40°W, N30°E	N28°W	6347 m; 8037 m	Clustering ≳≈ 250 m
CVL	N45°E	Tchaptchet et al., 2017	N45°E	–	–	–

geologic maps and DEMs, and from the SAMSE determined bandwidth estimate based directly on the observed vent locations. Obtained directions are generally consistent, the main limitation noted when using the SAMSE-derived orientations being that as a constant bandwidth is assumed across a field, multiple fault directions are likely to be (incorrectly) smoothed out (e.g., Biu).

The 'vents-to-events' method of Runge et al. (2014) was applied to each of the monogenetic volcanic fields in the CVL. However, the size and complexities of these fields resulted in significant issues when applying the original routine. The algorithm would not converge without an overly strict annealing schedule that essentially forced convergence to non-optimal solutions (local minima). This may be due to differences in structural controls between and within the fields and the limited number of documented multiple-vent events to tune the posterior distributions. Known multiple vent-events on the CVL include only two fissure eruptions on Mt. Cameroon (e.g., Suh et al., 2003) and some nested scoria cones in the Adamawa and Biu volcanic fields (for which evidence of contemporaneous formation is pending). But when these few events are used to update distributions for the entire set of volcanic fields, significant uncertainties are introduced.

Additional issues encountered include the sensitivity of the algorithm to volcanic field boundary definitions, buried vents (e.g., through subsequent lava flows and eruptive deposits from Mt. Cameroon; Marcel et al., 2018; Aka et al., 2018) and to the high potential for unidentified vents due to the moderate SRTM DEM resolution. This application presents an opportunity to highlight the limitations of the original code when applied to such complex regions, as well as the importance of tailoring prior distributions to a volcanic field of interest (e.g., via Bayesian methods).

4.3. Spatial organization of vents

In all volcanic fields (except for Oku), monogenetic vents find their nearest neighbor (NN) on average within a distance of <2000 m (Table 2; Fig. 3). The NN distributions are all positively skewed (1.16 for Tombel/Manengouba to 3.21 for Biu), and the kurtosis – indicating the presence of outliers – ranges between 1.1 (Tombel/Manengouba) and 16.4 (Mt. Cameroon).

The spatial distribution results show a gradual increase of the vent density from northeast to southwest along the CVL. This is in tandem with a reduction in the mean NN distances (Figs. 3 and 4). The areal densities are $>0.2\ km^{-2}$ for the Bioko and Mt. Cameroon fields, but drop substantially below this value for all other studied areas (Fig. 4a). It must be noted that the here reported spatial vent densities are based on the convex hull boundary definition as well as the number of identified vents. As both of these quantities are likely provided with inaccuracies, the calculated areal densities must be considered first-order approximations only.

The test statistics R (Clark and Evans, 1954), based on a convex hull boundary definition, suggests that the distribution of vents in all analyzed monogenetic volcanic fields is not consistent with a Poisson (random) distribution, but rather with a clustered arrangement (Fig. 4b). R values are between 0.40 (Biu) and 0.85 (Noun) with a tendency of stronger clustering (smaller R) for volcanic fields in the northern part of the CVL (Adamawa, Biu). While for volcanic fields containing >100 vents, the degree of clustering does not depend on the size of the dataset, it becomes more variable for volcanic fields with a smaller number of vents (see discussion in Cañón-Tapia, 2021). This is the case of the volcanic fields situated in the northern, continental part of the CVL (Noun, Oku, Adamawa, Biu; Fig. 4b). The spatial vent pattern closest to a random (Poisson) distribution is that of the Noun volcanic field.

Application of Ripley's $K(r)$ function to the Bioko, Noun and Biu volcanic fields (Fig. 5) shows generally strong clustering at almost all spatial scales, independent of the chosen boundary definition (convex hull, minimum area rectangle, minimum area ellipse, KDE). Random

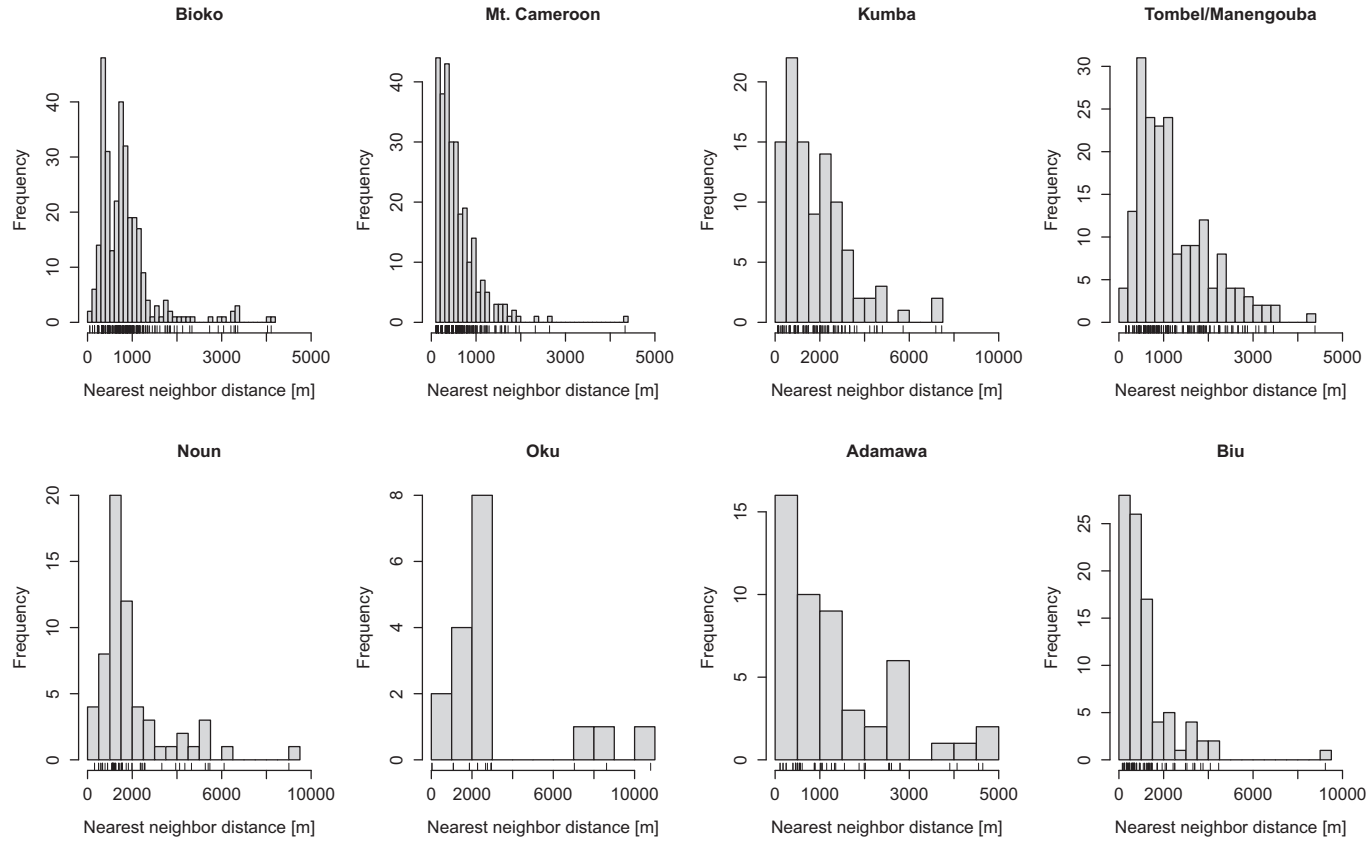

Fig. 3. Nearest neighbor histograms of vents of the eight analyzed monogenetic volcanic fields. Note that the abscissa is scaled to either 5000 m or 10,000 m for ease of comparison.

distribution of vents is observed only for $r < 200$–400 m (Bioko and Biu; all boundary definitions), while this threshold rises slightly to $r \sim 500$ m for the Biu volcanic field and the KDE boundary definition, primarily due to the smaller total area as compared to other boundaries. For the Noun volcanic field, vents are clustered for $r > 800$ m (minimum area rectangle), $r > 1100$ m (minimum area ellipse, KDE) and $r > 1200$ m (convex hull). Due to the shape of the Noun volcanic field, one can notice a slight influence of the boundary definition on the spatial scales at which clustering appears. Visual inspection of how these four boundaries fit the point data (Fig. 5) provides further insight into why these clustering algorithms are producing likely implausible results (e.g., irregular shapes that are unlikely to represent natural subsurface structures, large areas of empty space). It is also apparent that none of these four volcanic field boundaries are likely suitable for statistical clustering analysis as divergence from randomness at almost all distances is noted but not physically plausible. One potential exception to this is the convex hull of the Noun volcanic field (Fig. 5) where clustering is noted between 2000 and 4500 m. These values are close to the anisotropic SAMSE bandwidths for this volcanic field (Table 3).

The expert elicited prior distributions for eruption event length from Runge et al. (2014) imply a length in the order of 2000–4000 m. Hence, if events of this dimension were common within the observed vents on the CVL, we would expect to observe clustering at this distance (r). This is not apparent for any of the CVL volcanic fields, or for any of the four boundary definitions here (except for Noun with a convex hull as previously stated). However, these values are not that far from the SAMSE estimated bandwidths based on the observed vent locations. Table 3 includes the distances (r) above which clustering was calculated using a convex hull boundary, although given the discussion above it is noted that these values likely are uninformative.

4.4. Spatial hazard assessment using KDE

Kernel Density Estimates (KDEs) produced from the observed vent locations provide a non-parametric estimate of the spatial probability of future volcanic activity (Connor and Connor, 2009; Bebbington, 2013; Connor et al., 2019). The overall vent distribution indicates strongly clustered patterns under the conditional assumption of a convex hull field boundary (see Figs. 4b and 5). Spatial density estimates may offer new insights into the regional tectonic controls on vent locations and therefore into the underlying geological processes. Anisotropic kernel bandwidths resulting from the SAMSE approach cover the range from ~1.5 km (Mt. Cameroon) to ~8 km (Biu), while the degree of anisotropy varies among the studied volcanic fields (Table 3). The strike directions extracted from the bandwidth matrix show a marked change from ~N20°E–N40°E in the southwest to N20°W–N60°W in the northern sector of the CVL (Table 3). Except for the Noun volcanic field, these values are in rough agreement with the main or at least one of multiple strike directions obtained from geologic maps and DEMs (Nkono et al., 2009; Marcel et al., 2018; Njeudjang et al., 2020).

The percentile contour plots of the spatial density estimate for all monogenetic volcanic fields on the CVL are shown in Fig. 6. A comparable map displaying absolute spatial vent densities (in units m^{-2}) is included in the Supplementary Materials (Fig. S7).

The highest local vent densities are recorded at Mt. Cameroon ($>6 \times 10^{-3}$ km^{-2}), followed by the Bioko, Tombel/Manengouba and Adamawa volcanic fields ($>3 \times 10^{-3}$ km^{-2}). For the Bioko, Mt. Cameroon and Noun volcanic fields, the spatial density extends into the Atlantic Ocean and an adjacent lake (Lac Bamendjing), respectively. A special case is the Biu volcanic field which consists of three separate vent clusters, and the KDE results differ substantially, depending on whether the vents are

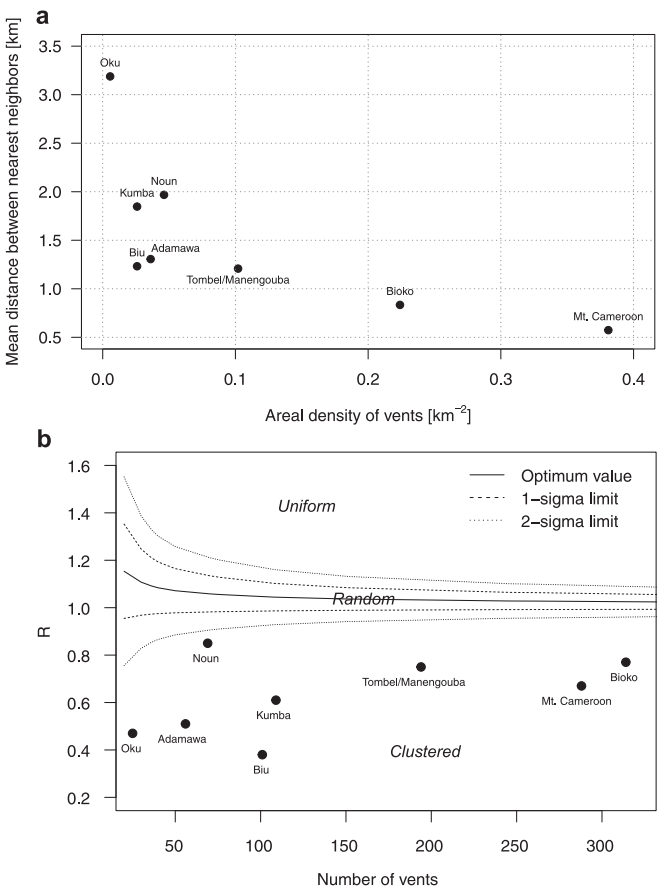

Fig. 4. (a) Mean nearest neighbor distance as a function of the areal vent density for the eight analyzed monogenetic volcanic fields. (b) Summary of the applied test statistics *R* (Clark and Evans, 1954) to infer the spatial distribution pattern (uniform, random, clustered) of vents along the Cameroon Volcanic Line, based on a convex hull boundary definition.

subdivided into three independent volcanic fields. The spatial density for the latter case results in high vent density values in the center of the subfield and a sharp decline of density beyond. Following a conservative approach, we therefore calculated the KDE for the entirety of vents in the Biu volcanic field, although the three subfields vary slightly in trending (Fig. 6). Due to the small number of vents, the results for the Oku volcanic field must be viewed with caution. Finally, the Mt. Cameroon and Kumba volcanic fields are located close to each other so that the spatial density isolines overlap (Fig. 6). Particularly in the northern part of the Mt. Cameroon volcanic field, the actual spatial density is thus likely to be higher than shown in Fig. 6.

4.5. Scoria cone dimensions

The scoria cone morphometry results show a wide range from <100 m to >1000 m in both the mean and median values of W_{co} (Fig. 7 and Table 4). Spatially, W_{co} increases from median values of 365–425 m in the southwest to 495–555 m in the northeastern part of the CVL (Fig. 7b). Results of the Tukey HSD post-hoc test show, for example, that the average W_{co} of cones in the Bioko and Mt. Cameroon volcanic fields are not significantly different from each other ($p = 0.21$), while the average W_{co} registered for Mt. Cameroon and Biu are highly significantly different ($p < 0.001$). All test results are compiled in Table S1 in the Supplementary Materials. Furthermore, the scatter of the W_{co} value varies among the volcanic fields. Although statistically not significant at 1σ uncertainty, there appears to be a trend of increasing eccentricity of scoria cones towards the northern part of the CVL (Fig. S6). For all volcanic fields except Adamawa, the mean value of W_{co} is larger than the median, indicating the distribution of W_{co} is positively skewed.

5. Discussion

5.1. New vent catalog for hazard assessment

We have located a total of 1156 vents, including 50 maars, along the CVL by analysis of DEMs, representing the most complete catalog so far of monogenetic vents in this area. It is apparent that vents are neither evenly/regularly nor randomly distributed across the CVL (Section 5.3), which is in line with the complex geologic and tectonic setting. The CVL comprises both polygenetic and monogenetic volcanoes on oceanic and continental crust and is characterized by changes in the stress regime along the ~1700 km long structure. Clustering on a larger scale was informed by previous geologic work and visual inspection to group these 1156 vents into their most likely volcanic field (of which we defined eight). However, the delineation of individual monogenetic volcanic fields as independent systems may inherently bias the results from statistical analyses. Ideally, such decisions should follow conceptual models of volcanism in a particular region (as far as these exist; Connor et al., 2019) or mathematical methods of cluster analyses (e.g., Everitt et al., 2011). Given that the application of such models is problematic to detect the most objective volcanic field boundaries (Runge et al., 2015; Cañón-Tapia, 2020), we defined individual fields based on geological/tectonic information and visual assessment of vent distribution. The vent catalog compiled here is presented as a starting database, with the hope that it will be improved by the community and used for own analyses and re-assessment.

Using our vent catalog, some preliminary analyses were undertaken to explore the spatial density of eruptive centers. The NN distances derived for the eight volcanic fields along the CVL vary from ~0.57 km (Mt. Cameroon) to ~3.2 km (Oku) with spatial density estimates spanning the range 5.6×10^{-3}–3.6×10^{-2} km^{-2} along the CVL. Both of these sets of values fit within previous work on global datasets (e.g., Le Corvec et al., 2013).

The KDE maps created in this study provide an initial estimate of spatial variations within the monogenetic fields of the CVL from Bioko to Adamawa and Biu. These absolute and relative spatial vent densities may provide a first-order approximation of the likely areas for future vent opening. As the SAMSE kernel estimator results to determine a field-wide optimized bandwidth based solely on observed vent locations align relatively well with the underlying independently determined stress fields, some confidence may be placed in conclusions around these vent locations being related to the underlying stress conditions (Table 3). However, the situation is more complicated in those monogenetic volcanic fields where multiple stress directions are observed.

5.2. Complexity of spatial distribution analysis

We used a variety of exploratory statistics including first-order (Clark-Evans), second-order (Ripley's *K*), and more nuanced methods, such as the vent-to-event method (Runge et al., 2014), and investigated the sensitivities of these results using four different field boundaries. The results are inconclusive, and the inspection of the vent distribution proved to be complex. In particular, as is commonly observed in volcanic field analysis, the definition of a field boundary is problematic and remains a large source of uncertainty. The main issue encountered here was the inclusion of the external-most vents (potential outliers), adding extra space and ultimately causing the appearance of vent clustering at all scales (Runge et al., 2015; Section 5.3; Fig. 5). This seems to strongly affect the convex hull, minimum area rectangle and minimum area ellipse boundaries, and to a slightly lesser extent the KDE boundaries. An exception is the Noun volcanic field where we found significant vent clustering for distances in between ~2.0 km and ~ 4.5 km for the convex hull boundary. Clustering at these dimensions matches the prior

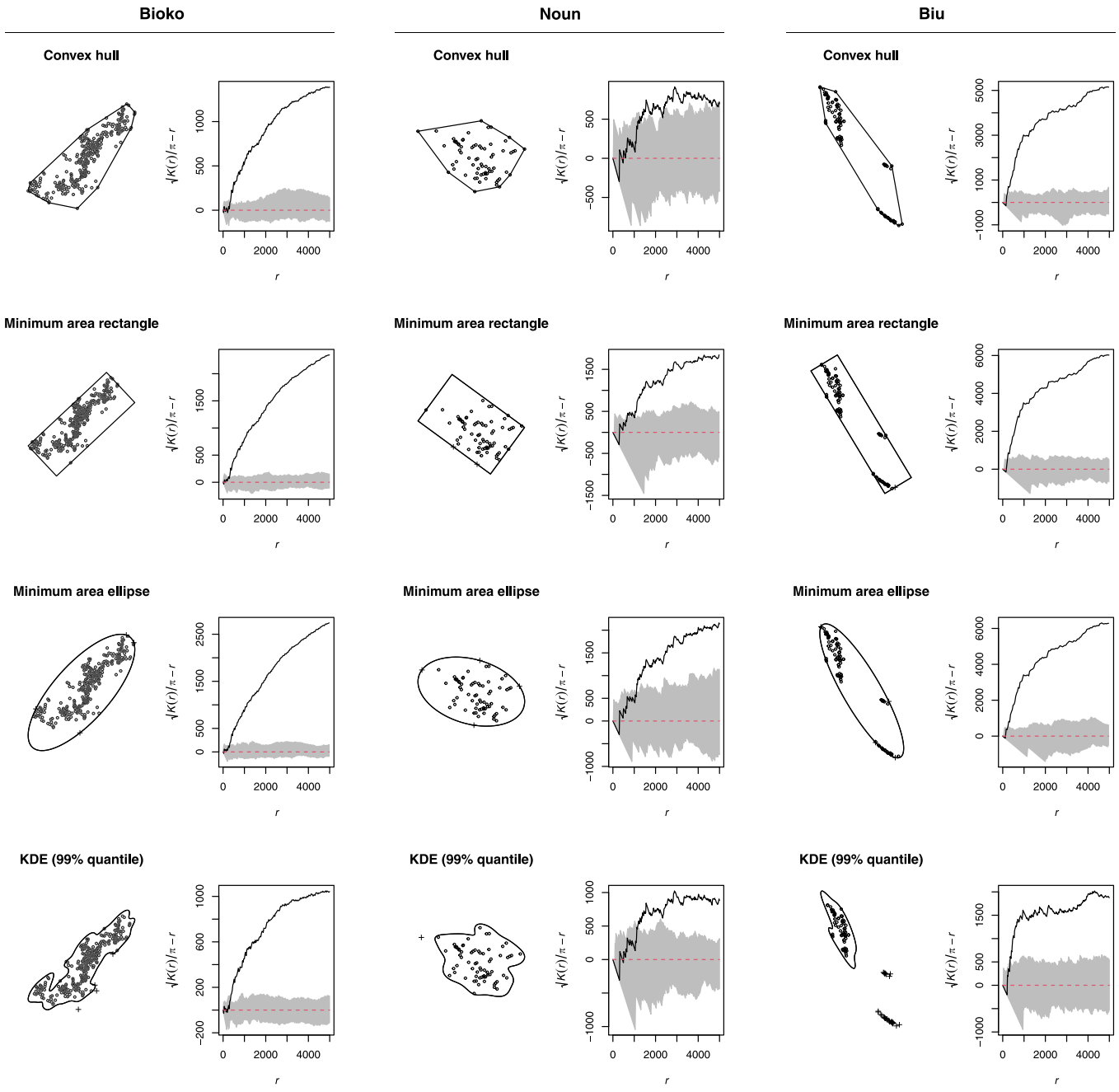

Fig. 5. Volcanic field boundary definitions and associated plots of $L - r$ against r for the Bioko, Noun and Biu volcanic fields. Stars indicate vents that are located at the field boundary or outside of the field. The grey areas define areas produced via Monte Carlo simulations within the defined volcanic field shapes to obtain the boundaries outside which a result may be assumed as statistically significant ($p \leq 0.05$), the black line shows the results from the actual vents.

distribution of event length set up by Runge et al. (2014) and could be informative for the processes controlling an eruptive event (e.g., tectonic environment, magma plumbing system, crustal settings). Our results suggest avoiding convex hull and minimum area rectangle/ellipse boundaries unless geologically justified, as these will inevitably lead to apparently clustered distributions. Thus, these area determination methods may be unsuitable for assessing spatial clustering in monogenetic volcanic fields, although they do provide a set of automated boundary definitions for necessary sensitivity analyses. KDE boundaries also caused problems in setting meaningful volcanic field boundaries (see the example of the Biu volcanic field), but may be performing better when it comes to addressing 'outlier' vents.

Future work related to spatial vent analyses could be directed towards estimating hidden/missing vents due to burial and the development of region-specific distributions of geometric event properties for 'vents-to-events' analyses. In this context, updating prior distributions with more multiple-vent events is paramount to group individual vents and thus avoid overestimation of spatial event density. Furthermore, the additional development of more flexible, non-parametric approaches to define field boundaries that may accommodate potential buried vents as well as the effect of field outliers is key (e.g., more flexible kernels where the bandwidth varies with location or age, or potentially both, see the spatio-temporal NN kernel of Connor and Hill, 1995). The example of the CVL has shown that statistical point-process analyses alone cannot account for the complexity of some volcanic settings and suggests that point-process assumptions should be replaced with new alternative

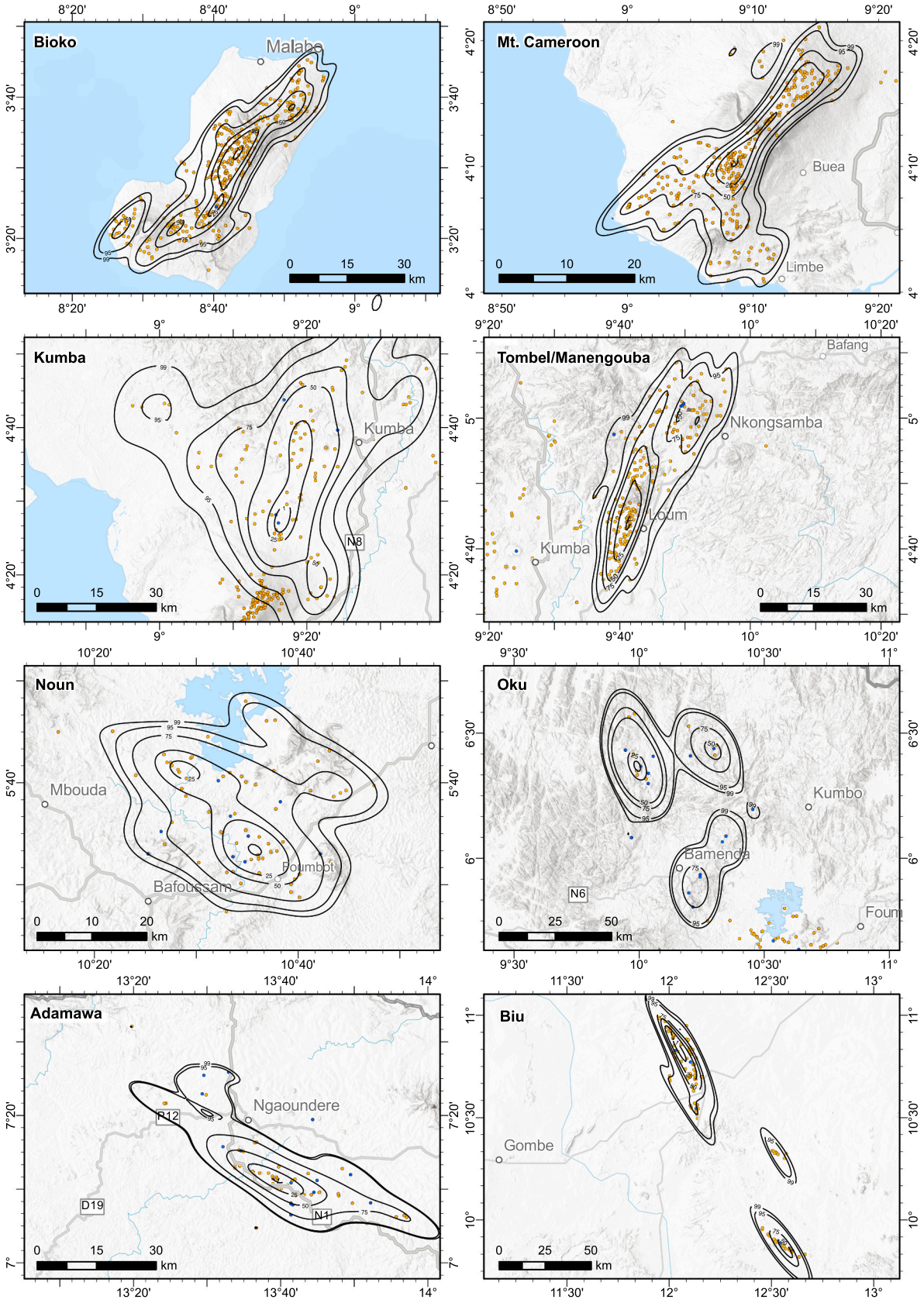

Fig. 6. Overview map of the eight studied volcanic fields along the Cameroon Volcanic Line, showing the probability of future vent formation, based on the KDE analysis of identified past eruption locations. Contours show the 1st, 25th, 50th, 75th, 95th and 99th percentiles. Kernel bandwidths used to construct the KDE are given in Table 3. Base map is the ArcGIS World Elevation Terrain layer with multi-directional hillshade. A map showing absolute vent density is given in Fig. S7.

hypotheses and accompanying methodologies to bridge this gap from these simple theoretical models to more complex knowledge-driven estimates.

5.3. Spatial organization and morphometry of vents influenced by the geodynamic setting

There is a statistically significant increase of W_{co} along the CVL from the Bioko and Mt. Cameroon volcanic fields to the northern branches at Adamawa and Biu (Fig. 7). The change in W_{co} correlates with the mean NN distances, which indicate magmatic/volcanic processes rather than erosion.

Based on the morphological data, Mt. Cameroon is an endmember. It has the smallest median W_{co} value of 395 m with narrow variation (Fig. 7), which can be interpreted to be due to the dominant fissure-fed eruption of basanites (e.g., 1999 eruptions; Suh et al., 2003), fed directly

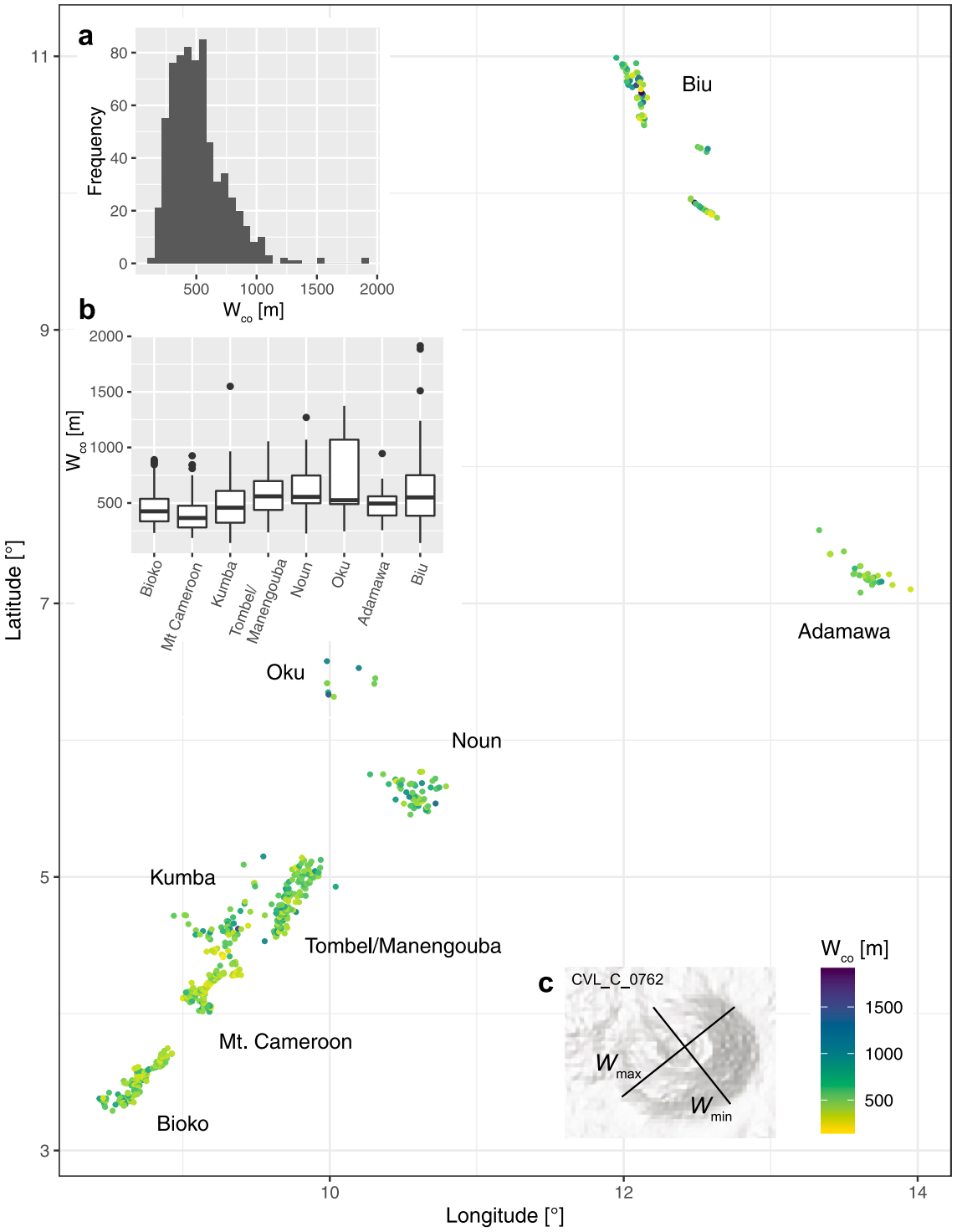

Fig. 7. Map of analyzed scoria cones along the Cameroon Volcanic Line. Monogenetic volcanic fields are indicated, and the color code refers to the average basal diameter W_{co}. Inset (a) shows a histogram of the registered average W_{co}; inset (b) displays boxplots of W_{co} for each volcanic field to visualize the trend of slightly increasing average diameter from south to north along the CVL; inset (c) illustrates the way the cone dimension was registered.

Table 4
Summary of results for estimating the basal diameter W_{co} for scoria cones in each monogenetic volcanic field (see Table 2 for number of cones in each field). The basal cone diameter is calculated as the average of the longest diameter W_{max} and shortest diameter W_{min}; the mean value of W_{co} for each volcanic field is given together with 1σ standard deviation. The median W_{co} is presented with the median absolute deviation. The eccentricity of the idealized ellipse is computed as $\sqrt{1-\frac{\left(\frac{W_{min}}{2}\right)^2}{\left(\frac{W_{max}}{2}\right)^2}}$ and is also cited with its 1σ standard deviation.

Volcanic field	Cones analyzed	Cones analyzed [%]	Mean W_{co} [m]	Median W_{co} [m]	Eccentricity
Bioko	139	44	464 ± 166	425 ± 141	0.48 ± 0.21
Mt. Cameroon	139	49	401 ± 158	365 ± 133	0.48 ± 0.20
Kumba	74	71	502 ± 249	458 ± 215	0.52 ± 0.17
Tombel/Manengouba	152	80	576 ± 188	560 ± 200	0.47 ± 0.20
Oku	9	82	728 ± 376	525 ± 415	0.46 ± 0.20
Noun	55	92	613 ± 224	555 ± 222	0.58 ± 0.18
Adamawa	31	74	489 ± 147	495 ± 126	0.54 ± 0.20
Biu	77	77	610 ± 351	550 ± 282	0.50 ± 0.21

from the HIMU-dominated source (e.g., Yokoyama et al., 2007; Wembenyui et al., 2020). This type of eruption produces relatively small cones and results in the smallest mean NN distance (~0.5 km) among all studied fields.

Another morphological endmember could be the Biu, Noun and Oku volcanic fields, and to lesser extent Adamawa (Table 4). Scoria cones in these volcanic fields tend to have larger W_{co} (>500 m), which may be due to more focused plumbing systems, as opposed to forming along fissures. This observation is further supported by our measured mean NN distances, being two to six times higher (~1.2–3.0 km) than in the Bioko and Mt. Cameroon volcanic fields. In other words, scoria cones in the northern part of the CVL are larger and spaced further apart (i.e., lower spatial density) than their counterparts in the southern sector.

The observed morphological changes broadly mimic the underlying crustal settings, where Bioko and Mt. Cameroon are located on the transitional oceanic-to-continental crust, while the rest of the studied fields developed on "true" continental crust. Crustal thickness has previously been invoked to explain vent distributions within monogenetic volcanic fields (e.g., Mazzarini, 2007), but the depth of the Moho does not change substantially across the CVL (Njiteu Tchoukeu et al., 2021). Our results further indicate that scoria cone morphology can also partially be influenced by underlying crustal settings, in conjunction with the magmatic properties (e.g., eruption styles, ascend speed, crustal contamination and geochemistry). Regarding the latter, it is interesting to note that isotopic variations in the continental part of the CVL have recently been documented to be large as opposed to the narrow variations at Bioko and Mt. Cameroon volcanics (see Asaah et al., 2015 for a review). This apparent correlation with the spatial vent pattern and morphologies requires further refinement as new topographic and geochemical data become available.

5.4. Accuracy and limitations

Remotely identifying surface features, such as scoria cones and phreatomagmatic volcanoes, on moderate resolution DEMs cannot replace field work (i.e., ground truthing), but constitutes a comparatively quick and inexpensive way to investigate large areas of volcanic activity. Consequently, the location catalog presented here is inherently incomplete, and needs to be updated as new data become available (e.g., global release of the 12 m TanDEM-X data). This incompleteness stems from (1) the spatial resolution and accuracy of the global DEM resources (Rodriguez et al., 2006), and (2) the burial and overprinting of older structures by new eruptions and degradation due to intense tropical erosion (e.g., Mt. Cameroon; Chauvel et al., 2005). Consequently, the dataset is biased towards the younger eruption products (see Aka et al., 2018). In particular, maars and tuff rings often act as local sedimentary basins, filling up with sediment and water and hampering remote identification of older maar and tuff ring structures (e.g., Rohrmüller et al., 2017). Hence, older phases of activity of monogenetic volcanic fields cannot be captured accurately using DEM-based mapping, particularly in irregular terrain (e.g., Oku volcanic field) and tropical climate. Due to a dearth of context information, it was not possible to conduct a quantitative analysis of missed vents (cf. Runge et al., 2014) or false positives. However, recent volcanic activity is the most relevant one for hazard assessment (e.g., Connor et al., 2000).

A lack of a suitable number of proven multi-vent eruptive events (e.g., a fissure eruption producing several vents at the same time; Suh et al., 2003) for the CVL impeded a robust estimation of volcanic events in relation to the identified cones and maars. Even if such data will be available, new approaches (as compared to that by Runge et al., 2014) must be developed, considering the complexity of volcanism and its tectonic control along the CVL (e.g., Adams, 2022).

Benchmarking our dataset against published (Piper and Richardson, 1972; Nkono et al., 2009) spatial distributions indicates omission of ~25% and ~ 1% of vents within the Bioko and Tombel/Manengouba volcanic fields, respectively. Our mapping has also identified 70 new vents (~36% of the total number) within the Tombel/Manengouba volcanic field. This exercise gives a sense of the uncertainties regarding the number and completeness of the vent catalog and how it might evolve in the course of regionally focused fieldwork.

In addition to the new approaches required for the assessment of vent distribution and spatial density in the study area, future work should include the extension of the existing catalog of vent locations with temporal information on eruption ages to estimate recurrence rates (Lapi et al., 2010; Ntepe et al., 2019). This is at best patchy for the CVL due to the lack of accurate chronologic data (Aka et al., 2018). Therefore, it appears imperative to date the emplacement of further monogenetic volcanoes by radiometric techniques. Whereas K/Ar and $^{40}Ar/^{39}Ar$ techniques are associated with high uncertainty levels at Late Pleistocene and Holocene timescales (e.g., Mertz et al., 2015), luminescence methods or cosmogenic nuclides such as ^{3}He, ^{10}Be and ^{21}Ne are capable of producing accurate and precise chronologies in such contexts (e.g., Aka et al., 2009; Heineke et al., 2016; Richter et al., 2017; Schmidt et al., 2017a, 2017b). Given the number of eruptive vents deduced in this study, a detailed temporal eruption record of each of them is out of scope in the future. By exploiting the age-dependent morphological degradation of volcanic structures (e.g., scoria cones), relative chronologies can be developed at large scale, although a range

of complicating factors should be considered (e.g., Kervyn et al., 2012; Kereszturi et al., 2013; Vörös et al., 2021). For instance, some recent studies have shown the potential of morphometric analyses of terrestrial and extraterrestrial volcanic edifices for deriving their relative age using DEMs (e.g., Zarazúa-Carbajal and De la Cruz-Reyna, 2020).

6. Conclusions

We compiled a catalog of vent locations (mainly scoria cones and maars) on eight monogenetic volcanic fields along the CVL by combining DEM and satellite imagery analyses with field work. Benchmarking against two other datasets of mapped scoria cones indicates varying accuracy of between 75% and 99%, with main limitations imposed by DEM resolution and highly eroded or buried vents. Vent-to-event collapsing for all eight monogenetic volcanic fields was impeded by insufficient information to tune posterior information. To test for non-random vent distribution patterns revealing controlling factors on (future) eruption locations, we analyzed NN distances, spatial vent density using KDE and conducted randomness test statistics, including the results' sensitivity to volcanic field boundary definition. We find that all monogenetic volcanic fields on the CVL show a clustered vent distribution, independent of the chosen boundary definition. From a hazard assessment perspective, however, it appears that convex hull as well as rectangular and elliptical boundaries are generally unsuitable, as they disregard internal structures within a volcanic field and unrealistically imply zero eruption probability just outside the field boundaries. KDE boundary definitions seem more promising, although they require further methodological development to account for the specific setting of this study. The point pattern analyses demonstrate that monogenetic volcanism on the CVL and underlying magmatic and tectonic forcing are much more complex than in many other monogenetic volcanic provinces.

Finally, we find that scoria cone basal diameter and vent distribution match well with the documented geochemical/isotopic variation, with more mafic eruptions at Bioko and Mt. Cameroon producing parasitic rows of smaller craters (multi-vent events) with higher spatial density, and larger single edifices (single-vent events) with lower spatial density towards the north. As crustal thickness and the overall extensional tectonic regime are more or less uniform across the entire CVL (Tedla et al., 2011; Njome and de Wit, 2014, and references therein; Njiteu Tchoukeu et al., 2021), it can be speculated that the scoria cone geometry is mainly a function of magma geochemical composition and the occurrence of favorable structures and/or tectonic stress conditions allowing magma ascent (Corazzato and Tibaldi, 2006).

In future work, the available toolkits for point pattern analyses, vent-to-event collapsing and volcanic field boundary definition should be further developed to account for the special setting of the CVL characterized by an ocean-continent transition and multiple stress directions. Finally, for quantifying recurrence rates of monogenetic eruptions, numeric ages for at least suitable subsets of all vents should be generated.

CRediT authorship contribution statement

C. Schmidt: Conceptualization, Investigation, Formal analysis, Visualization, Writing – Original draft, Project administration, Funding acquisition. C. Laag: Investigation, Software, Validation, Data curation, Writing – Review and Editing. M. Whitehead: Conceptualization, Software, Formal analyses, Writing – Original draft. J. Profe: Software, Validation, Data curation, Writing – Review and Editing. F. Aka: Validation, Data curation, Writing – Review and Editing. T. Hasegawa: Validation, Data curation, Writing – Review and Editing. G. Kereszturi: Conceptualization, Formal analyses, Writing – Original draft.

Declaration of Competing Interest

The authors declare that they have no known competing financial interests or personal relationships that could have appeared to influence the work reported in this paper.

Acknowledgments

We wish to thank Prof. Jean-Pierre Tchouankoue (University of Yaoundé I) for the warm welcome in Cameroon, logistic support and fruitful discussions. The field trip by CS to Cameroon was financed by the German Research Foundation (Deutsche Forschungsgemeinschaft) under the grant number SCHM3051/7-1. Furthermore, we are grateful for helpful scientific exchange with Prof. Benjamin van Wyk de Vries (University of Clermont-Ferrand) in the early stage of this study. Finally, many thanks go to the two anonymous reviewers of this paper for supportive and helpful comments. This is IPGP contribution number 4266.

Appendix A. Supplementary data

Supplementary data to this article can be found online at https://doi.org/10.1016/j.jvolgeores.2022.107558.

References

Adams, A., 2022. Insights into the source of magmatic hot-lines: forty years of geophysical studies of the Cameroon Volcanic Line. Front. Earth Sci. 10, 838993.
Aka, F.T., 2000. Noble gas Systematics and K-Ar Chronology: Implications for the Geochemical and Geotectonic Evolution of the Cameroon Volcanic Line, West Africa. Doctoral Thesis. Okayama University, Okayama.
Aka, F.T., Yokoyama, T., 2012. Current status of the debate about the age of Lake Nyos dam (Cameroon) and its bearing on potential flood hazards. Nat. Hazards 65, 875–885.
Aka, F.T., Nagao, K., Kusakabe, M., Sumino, H., Tanyileke, G., Ateba, B., Hell, J., 2004. Symmetrical Helium isotope distribution on the Cameroon Volcanic Line, West Africa. Chem. Geol. 203, 205–223.
Aka, F.T., Yokoyama, T., Kusakabe, M., Nakamura, E., Tanyileke, G., Ateba, B., Ngako, V., Nnange, J., Hell, J., 2008. U-series dating of Lake Nyos maar basalts, Cameroon (West Africa): Implications for potential hazards on the Lake Nyos dam. J. Volcanol. Geotherm. Res. 176, 212–224.
Aka, F.T., Nagao, K., Kusakabe, M., Nfomou, N., 2009. Cosmogenic helium and neon in mantle xenoliths from the Cameroon Volcanic Line (West Africa): preliminary observations. J. Afr. Earth Sci. 55, 175–184.
Aka, F.T., Hasegawa, T., Nche, L.A., Asaah, A.N.E., Mimba, E.M., Teitchou, I., Ngwa, C., Miyabuchi, Y., Kobayashi, T., Kankeu, B., Yokoyama, T., Tanyileke, G., Ohba, T., Hell, J.V., 2018. Upper Triassic mafic dykes of Lake Nyos, Cameroon (West Africa) I: K-Ar age evidence within the context of Cameroon Line magmatism, and the tectonic significance. J. Afr. Earth Sci. 141, 49–59.
Asaah, A.N.E., Yokoyama, T., Aka, F.T., Usui, T., Wirmvem, M.J., Tchamabe, B.C., Ohba, T., Tanyileke, G., Hell, J.V., 2015. A comparative review of petrogenetic processes beneath the Cameroon Volcanic Line: Geochemical constraints. Geosci. Front. 6, 557–570.
Ateba, B., Dorbath, C., Dorbath, L., Ntepe, N., Frogneux, M., Aka, F.T., Hell, J.V., Delmond, J.C., Manguelle, D., 2009. Eruptive and earthquake activities related to the 2000 eruption of Mount Cameroon volcano (West Africa). J. Volcanol. Geotherm. Res. 179, 206–216.
Awé, W.S., Tchameni, R., Dawaï, D., Kepnamou, A.D., Danra, M.D.G.B., Haskand, K.J., Gaoussou, B., Sini, A., 2021. Morphotectonic Analysis of Mboula Area in Relation with Central Cameroon Shear Zone (CCSZ) and Lithology using Remote Sensing and Field Data. J. Geosci. Geomat. 9, 83–95.
Barfod, D.N., Fitton, J.G., 2014. Pleistocene volcanism on São Tomé, Gulf of Guinea, West Africa. Quat. Geochronol. 21, 77–89.
Baudin, P., 1991. Le magmatisme Mesozoique a Cenozoique du fosse de la Benoue (Nigeria). Geochronologie, Petrogenese, Cadre geodynamique. PhD thesis. Universite de Droit d'Economie et des Sciences d'Aix-Marseille, France.
Bebbington, M.S., 2013. Assessing spatio-temporal eruption forecasts in a monogenetic volcanic field. J. Volcanol. Geotherm. Res. 252, 14–28.
Bebbington, M., 2015. Spatio-volumetric hazard estimation in the Auckland volcanic field. Bull. Volcanol. 77, 1–15.
Brown, S.K., Sparks, R.S.J., Mee, K., Vye-Brown, C., Ilyinskaya, E., Jenkins, S.F., Loughlin, S.C., 2015. Appendix B – Region 2: country and regional profiles of volcanic hazard and risk: Africa and Red Sea. In: Loughlin, S.C., Sparks, R.S.J., Brown, S.K., Jenkins, S.F., Vye-Brown, C. (Eds.), Global Volcanic Hazards and Risk. Cambridge University Press, Cambridge.
Burke, K., 2001. Origin of the Cameroon Line of Volcano-Capped Swells. J. Geol. 109, 349–362.

Cañón-Tapia, E., 2020. Influence of method selection on clustering analyses of point-like features: examples from three zones of distributed volcanism. Geomorphology 354, 107063.
Cañón-Tapia, E., 2021. Vent distribution and sub-volcanic systems: Myths, fallacies, and some plausible facts. Earth Sci. Rev. 221, 103768.
Chako Tchamabé, B., Ohba, T., Issa, Ooki, Youmen, D., Owona, S., Tanyileke, G., Hell, J. V., 2014. Temporal evolution of the Barombi Mbo Maar, a polygenetic maar-diatreme volcano of the Cameroon Volcanic Line. Int. J. Geosci. 5, 1315–1323.
Chauvel, C., Diaa, A.N., Bulourde, M., Chabaux, F., Durand, S., IIdefonse, P., Gerard, M., Deruelle, B., Ngounouno, I., 2005. Do decades of tropical rainfall affect the chemical compositions of basaltic lava flows in Mount Cameroon? J. Volcanol. Geotherm. Res. 141, 195–223.
Clark, P.J., Evans, F.C., 1954. Distance to nearest neighbor as a measure of spatial relationships in populations. Ecology 35, 445–453.
Condit, C.D., Connor, C.B., 1996. Recurrence rates of volcanism in basaltic volcanic fields: an example from the Springerville volcanic field, Arizona. Geol. Soc. Am. Bull. 108, 1225–1241.
Connor, C.B., Connor, L.J., 2009. Estimating spatial density with kernel methods. In: Connor, C.B., Chapmen, N.A., Connor, L.J. (Eds.), Volcanic and Tectonic Hazard Assessment for Nuclear Facilities. Cambride University Press, Cambridge, pp. 346–368.
Connor, C.B., Hill, B.E., 1995. Three nonhomogeneous Poisson models for the probability of basaltic volcanism: application to the Yucca Mountain region, Nevada. J. Geophys. Res. Solid Earth 100, 10107–10125.
Connor, C.B., Stamatakos, J.A., Ferrill, D.A., Hill, B.E., Ofoegbu, G.I., Conway, F.M., Sagar, B., Trapp, J., 2000. Geologic factors controlling patterns of small-volume basaltic volcanism: Application to a volcanic hazards assessment at Yucca Mountain, Nevada. J. Geophys. Res. Solid Earth 105, 417–432.
Connor, L.J., Connor, C.B., Meliksetian, K., Savov, I., 2012. Probabilistic approach to modeling lava flow inundation: a lava flow hazard assessment for a nuclear facility in Armenia. J. Appl. Volcanol. 1, 1–19.
Connor, C.B., Connor, L., Germa, A., Richardson, J., Bebbington, M., Gallant, E., Saballos, A., 2019. How to use kernel density estimation as a diagnostic and forecasting tool for distributed volcanic vents. Stat. Volcanol. 4, 1–25.
Corazzato, C., Tibaldi, A., 2006. Fracture control on type, morphology and distribution of parasitic volcanic cones: an example from Mt. Etna, Italy. J. Volcanol. Geotherm. Res. 158, 177–194.
Cornen, G., Bande, Y., Giresse, P., Maley, J., 1992. The nature and chronostratigraphy of Quaternary pyroclastic accumulations from lake Barombi Mbo (West-Cameroon). J. Volcanol. Geotherm. Res. 51, 357–374.
Del Negro, C., Cappello, A., Neri, M., Bilotta, G., Hérault, A., Ganci, G., 2013. Lava flow hazards at Mount Etna: constraints imposed by eruptive history and numerical simulations. Sci. Rep. 3, 1–8.
Déruelle, B., Moreau, C., Nkoumbou, C., Kambou, R., Lissom, J., Njonfang, E., Ghogomu, R.T., Nono, A., 1991. The Cameroon Line: a review. In: Kampunzu, A.B., Lubala, R.T. (Eds.), Magmatism in Extensional Structural Settings. Springer, Berlin, Heidelberg.
Déruelle, B., Ngounouno, I., Demaiffe, D., 2007. The 'Cameroon Hot Line' (CHL): a unique example of active alkaline intraplate structure in both oceanic and continental lithospheres. Compt. Rendus Geosci. 339, 589–600.
Dóniz, J., Romero, C., Carmona, J., García, A., 2011. Erosion of cinder cones in Tenerife by gully formation, Canary Islands, Spain. Phys. Geogr. 32, 139–160.
Dóniz-Páez, J., 2015. Volcanic geomorphological classification of the cinder cones of Tenerife (Canary Islands, Spain). Geomorphology 228, 432–447.
Everitt, B.S., Landau, S., Leese, M., Stahl, D., 2011. Cluster Analysis. John Wiley & Sons. Ltd., New York, p. 330.
Fitton, J.G., 1987. The Cameroon line, West Africa: a comparison between oceanic and continental alkaline volcanism. Geol. Soc. Lond. Spec. Publ. 30, 273–291.
Fitton, J.G., Dunlop, H.M., 1985. The Cameroon line, West Africa, and its bearing on the origin of oceanic and continental alkali basalt. Earth Planet. Sci. Lett. 72, 23–38.
Fornaciai, A., Favalli, M., Karátson, D., Tarquini, S., Boschi, E., 2012. Morphometry of scoria cones, and their relation to geodynamic setting: a DEM-based analysis. J. Volcanol. Geotherm. Res. 217-218, 56–72.
Freeth, S.J., Kay, R.L.F., 1987. The Lake Nyos gas disaster. Nature 325, 104–105.
Freeth, S.J., Rex, D.C., 2000. Constraints on the age of Lake Nyos, Cameroon. J. Volcanol. Geotherm. Res. 97, 261–269.
Graettinger, A.H., 2018. Trends in maar crater size and shape using the global Maar Volcano Location and Shape (MaarVLS) database. J. Volcanol. Geotherm. Res. 357, 1–13.
Grosse, P., Ochi Ramacciotti, M.L., Escalante Fochi, F., Guzmán, S., Orihashi, Y., Sumino, H., 2020. Geomorphology, morphometry, spatial distribution and ages of mafic monogenetic volcanoes of the Peinado and Incahuasi fields, southernmost Central Volcanic Zone of the Andes. J. Volcanol. Geotherm. Res. 401, 106966.
Guilbaud, M.-N., Siebe, C., Agustín-Flores, J., 2009. Eruptive style of the young high-Mg basaltic-andesite Pelagatos scoria cone, southeast of México City. Bull. Volcanol. 71, 859–880.
Guilbaud, M.-N., Siebe, C., Layer, P., Salinas, S., 2012. Reconstruction of the volcanic history of the Tacámbaro-Puruarán area (Michoacán, México) reveals high frequency of Holocene monogenetic eruptions. Bull. Volcanol. 74, 1187–1211.
Haag, M.B., Baez, W.A., Sommer, C.A., Arnosio, J.M., Filipovich, R.E., 2019. Geomorphology and spatial distribution of monogenetic volcanoes in the southern Puna Plateau (NW Argentina). Geomorphology 342, 196–209.
Heineke, C., Niedermann, S., Hetzel, R., Akal, C., 2016. Surface exposure dating of Holocene basalt flows and cinder cones in the Kula volcanic field (Western Turkey) using cosmogenic ^{3}He and ^{10}Be. Quat. Geochronol. 34, 81–91.
Issa, Ohba, Tchamabé, C.B., Padrón, E., Hernández, P., Eneke Takem, E.G., Barrancos, J., Sighomnoun, D., Ooki, S., Nkamdjou, S., Kusakabe, M., Yoshida, Y., Dionis, S., 2014. Gas emission from diffuse degassing structures (DDS) of the Cameroon volcanic line (CVL): Implications for the prevention of CO_2-related hazards. J. Volcanol. Geotherm. Res. 283, 82–93.
Jacquemin, H., Sheppard, S.M.F., Vidal, P., 1982. Isotopic geochemistry (O, Sr, Pb) of the Golda Zuelva and Mboutou anorogenic complexes, North Cameroun: mantle origin with evidence for crustal contamination. Earth Planet. Sci. Lett. 61, 97–111.
Kagou Dongmo, A., Wandji, P., Pouclet, A., Vicat, J.-P., Cheilletz, A., Nkouathio, D.G., Alexandrov, P., Tchoua, F.M., 2001. Évolution volcanologique du mont Manengouba (Ligne du Cameroun) ; nouvelles données pétrographiques, géochimiques et géochronologiques. C. R. Acad. Sci. Ser. IIA Earth Planet. Sci. 333, 155–162.
Kagou Dongmo, A., Nkouathio, D., Pouclet, A., Bardintzeff, J.-M., Wandji, P., Nono, A., Guillou, H., 2010. The discovery of late Quaternary basalt on Mount Bambouto: Implications for recent widespread volcanic activity in the southern Cameroon Line. J. Afr. Earth Sci. 57, 96–108.
Kamgang, P., Chazot, G., Njonfang, E., Tchoua, F., 2008. Geochemistry and geochronology of mafic rocks from Bamenda Mountains (Cameroon): source composition and crustal contamination along the Cameroon Volcanic Line. Compt. Rendus Geosci. 340, 850–857.
Kamgang, P., Njonfang, E., Nono, A., Dedzo, M.G., Tchoua, F.M., 2010. Petrogenesis of a silicic magma system: Geochemical evidence from Bamenda Mountains, NW Cameroon, Cameroon Volcanic Line. J. Afr. Earth Sci. 58, 285–304.
Kereszturi, G., Németh, K., 2016. Post-eruptive sediment transport and surface processes on unvegetated volcanic hillslopes–a case study of Black Tank scoria cone, Cima Volcanic Field, California. Geomorphology 267, 59–75.
Kereszturi, G., Jordan, G., Németh, K., Dóniz-Páez, J.F., 2012. Syn-eruptive morphometric variability of monogenetic scoria cones. Bull. Volcanol. 74, 2171–2185.
Kereszturi, G., Geyer, A., Martí, J., Németh, K., Dóniz-Páez, F.J., 2013. Evaluation of morphometry-based dating of monogenetic volcanoes—a case study from Bandas del Sur, Tenerife (Canary Islands). Bull. Volcanol. 75, 734.
Kereszturi, G., Bebbington, M., Németh, K., 2017. Forecasting transitions in monogenetic eruptions using the geologic record. Geology 45, 283–286.
Kervyn, M., Ernst, G.G.J., Carracedo, J.C., Jacobs, P., 2012. Geomorphometric variability of "monogenetic" volcanic cones: evidence from Mauna Kea, Lanzarote and experimental cones. Geomorphology 136, 59–75.
Kling, G.W., Clark, M.A., Wagner, G.N., Compton, H.R., Humphrey, A.M., Devine, J.D., Evans, W.C., Lockwood, J.P., Tuttle, M.L., Koenigsberg, E.J., 1987. The 1986 Lake Nyos gas disaster in Cameroon, West Africa. Science 236, 169–175.
Konfor, N., Temdjim, R., Richard, C., Ghogomu, N., Tchuitchou, R., Ajonina, H., 2007. Geochemistry of tertiary-quaternary lavas of Mt. Oku, Northwest Cameroon. Rev. Facult. Ingen. 40, 59–75.
Lapi, P.N., Ofoma, A.E., Amobi, J.O., Ngah, S.A., Ichiaghanam, O.I., 2010. Geostatistical prediction of future volcanic eruption and risk assessment for the Mount Cameroon volcano. Global J. Pure Appl. Sci. 16, 115–128.
Lar, U.A., Lekmang, I.C., Shuaibu, M.T., Mahmud, U.M., Yakubu, T.A., 2013. Volcanoes of Nigeria: a preliminary study. In: 7th Conference on African Geology, Assiut, Egypt.
Le Corvec, N., Spörli, K.B., Rowland, J., Lindsay, J., 2013. Spatial distribution and alignments of volcanic centers: Clues to the formation of monogenetic volcanic fields. Earth Sci. Rev. 124, 96–114.
Lee, D.C., 1994. A Chemical Isotopic and Geochronological Study of the Cameroon Line, West Africa. PhD thesis. University of Michigan, 179 p.
Lockwood, J.P., Rubin, M., 1989. Origin and age of the Lake Nyos maar, Cameroon. J. Volcanol. Geotherm. Res. 39, 117–124.
Lutz, T.M., Gutmann, J.T., 1995. An improved method for determining and characterizing alignments of pointlike features and its implications for the Pinacate volcanic field, Sonora, Mexico. J. Geophys. Res. Solid Earth 100, 17659–17670.
Maley, J., Livingstone, D.A., Giresse, P., Thouveny, N., Brenac, P., Kelts, K., Kling, G., Stager, C., Haag, M., Fournier, M., Bandet, Y., Williamson, D., Zogning, A., 1990. Lithostratigraphy, volcanism, paleomagnetism and palynology of Quaternary lacustrine deposits from Barombi Mbo (West Cameroon): preliminary results. J. Volcanol. Geotherm. Res. 42, 319–335.
Maluski, H., Coulon, C., Popoff, M., Baudin, P., 1995. ^{40}Ar/^{39}Ar chronology, petrology and geodynamic setting of Mesozoic to early Cenozoic magmatism from the Benue Trough, Nigeria. J. Geol. Soc. 152, 311–326.
Manville, V., 2010. An overview of break-out floods from intracaldera lakes. Glob. Planet. Chang. 70, 14–23.
Marcel, J., Abate Essi, J.M., Njandjock Nouck, P., Sanda, O., Manguelle-Dicoum, 2018. Validation of gravity data from the geopotential field model for subsurface investigation of the Cameroon Volcanic Line (Western Africa). Earth Planets Space 70, 42.
Marzocchi, W., Bebbington, M.S., 2012. Probabilistic eruption forecasting at short and long time scales. Bull. Volcanol. 74, 1777–1805.
Marzoli, A., Renne, P.R., Piccirillo, E.M., Francesca, C., Bellieni, G., Melfi, A.J., Nyobe, J. B., N'ni, J., 1999. Silicic magmas from the continental Cameroon Volcanic Line (Oku, Bambouto and Ngaoundere): ^{40}Ar-^{39}Ar dates, petrology, Sr-Nd-O isotopes and their petrogenetic significance. Contrib. Mineral. Petrol. 135, 133–150.
Marzoli, A., Piccirillo, E.M., Renne, P.R., Bellieni, G., Iacumin, M., Nyobe, J.B., Tongwa, A.T., 2000. The Cameroon Volcanic Line Revisited: Petrogenesis of Continental Basaltic Magmas from Lithospheric and Asthenospheric Mantle sources. J. Petrol. 41, 87–109.
Mazzarini, F., 2007. Vent distribution and crustal thickness in stretched continental crust: the case of the Afar Depression (Ethiopia). Geosphere 3, 152–162.

Mertz, D.F., Löhnertz, W., Nomade, S., Pereira, A., Prelević, D., Renne, P.R., 2015. Temporal–spatial evolution of low-SiO_2 volcanism in the Pleistocene West Eifel volcanic field (West Germany) and relationship to upwelling asthenosphere. J. Geodyn. 88, 59–79.
Montigny, R., Ngounouno, I., Déruelle, B., 2004. Âges K-Ar des roches magmatiques du fossé de Garoua (Cameroun) : leur place dans le cadre de la « Ligne du Cameroun ». Compt. Rendus Geosci. 336, 1463–1471.
Moreau, C., Regnoult, J.M., Déruelle, B., Robineau, B., 1987. A new tectonic model for the Cameroon Line, Central Africa. Tectonophysics 141, 317–334.
Moundi, A., Wandji, P., Bardintzeff, J.-M., Ménard, J.-J., Okomo Atouba, L.C., Mouncherou, O.F., Reusser, É., Bellon, H., Tchoua, F.M., 2007. Les basaltes éocènes à affinité transitionnelle du plateau Bamoun, témoins d'un réservoir mantellique enrichi sous la ligne volcanique du Cameroun. Compt. Rendus Geosci. 339, 396–406.
Németh, K., Kereszturi, G., 2015. Monogenetic volcanism: personal views and discussion. Int. J. Earth Sci. 104, 2131–2146.
Ngwa, C.N., Hansteen, T.H., Devey, C.W., van der Zwan, F.M., Suh, C.E., 2017. Origin and evolution of primitive melts from the Debunscha Maar, Cameroon: Consequences for mantle source heterogeneity within the Cameroon Volcanic Line. Lithos 288-289, 326–337.
Nieto-Torres, A., Martin Del Pozzo, A.L., 2019. Spatio-temporal hazard assessment of a monogenetic volcanic field, near México City. J. Volcanol. Geotherm. Res. 371, 46–58.
Njeudjang, K., Abate Essi, J.M., Kana, J.D., Teikeu, W.A., Njandjock Nouck, P., Djongyang, N., Tchinda, R., 2020. Gravity investigation of the Cameroon Volcanic Line in Adamawa region: Geothermal features and structural control. J. Afr. Earth Sci. 165, 103809.
Njiteu Tchoukeu, C.D., Basseka, C.A., Djomani, Y.P., Rousse, S., Etame, J., Llubes, M., Seoane, L., Som Mbang, C., Eyike Yomba, A., 2021. Crustal thickness, depth to the bottom of magnetic sources and thermal structure of the crust from Cameroon to Central African Republic: preliminary results for a better understanding of the origin of the Bangui magnetic Anomaly. J. Afr. Earth Sci. 179, 104206.
Njome, M.S., de Wit, M.J., 2014. The Cameroon Line: analysis of an intraplate magmatic province transecting both oceanic and continental lithospheres: constraints, controversies and models. Earth Sci. Rev. 139, 168–194.
Njome, M.S., Suh, C.E., Sparks, R.S.J., Ayonghe, S.N., Fitton, J.G., 2008. The Mount Cameroon 1959 compound lava flow field: morphology, petrography and geochemistry. Swiss J. Geosci. 101, 85–98.
Nkono, C., Féménias, O., Demaiffe, D., 2009. Geodynamic framework of large volcanic fields highlighted by SRTM DEMs: method evaluation and perspectives exampled on three areas from the Cameroon Volcanic Line. J. Volcanol. Geotherm. Res. 187, 13–25.
Nkouathio, D.G., Kagou Dongmo, A., Bardintzeff, J.M., Wandji, P., Bellon, H., Pouclet, A., 2008. Evolution of volcanism in graben and horst structures along the Cenozoic Cameroon Line (Africa): implications for tectonic evolution and mantle source composition. Mineral. Petrol. 94, 287–303.
Ntepe, N., Ngwa, C.N., Mbassa, B.J., Teichou, M.I., Ateba, B., 2019. Forecasting future volcanic eruptions at Mount Cameroon within the time interval 2000–2200. Bull. Volcanol. 81, 36.
Ort, M.H., Elson, M.D., Anderson, K.C., Duffield, W.A., Hooten, J.A., Champion, D.E., Waring, G., 2008. Effects of scoria-cone eruptions upon nearby human communities. Geol. Soc. Am. Bull. 120, 476–486.
Pedrazzi, D., Kereszturi, G., Lobo, A., Geyer, A., Calle, J., 2020. Geomorphology of the post-caldera monogenetic volcanoes at Deception Island, Antarctica — implications for landform recognition and volcanic hazard assessment. J. Volcanol. Geotherm. Res. 402, 106986.
Piper, J.D.A., Richardson, A., 1972. The Palaeomagnetism of the Gulf of Guinea Volcanic Province, West Africa. Geophys. J. Int. 29, 147–171.
Pouclet, A., Kagou Dongmo, A., Bardintzeff, J.-M., Wandji, P., Chakam Tagheu, P., Nkouathio, D., Bellon, H., Ruffet, G., 2014. The Mount Manengouba, a complex volcano of the Cameroon Line: volcanic history, petrological and geochemical features. J. Afr. Earth Sci. 97, 297–321.
R Core Team, 2021. R: A Language and Environment for Statistical Computing. R Foundation for Statistical Computing, Vienna, Austria. https://www.R-project.org/.
Richter, D., Klinger, P., Schmidt, C., van den Bogaard, P., Zöller, L., 2017. New chronometric age estimates for the context of the Neanderthal from Wannen-Ochtendung (Germany) by TL and argon dating. J. Archaeol. Sci. Rep. 14, 127–136.
Ripley, B.D., 1979. Tests of 'randomness' for spatial point patterns. J. R. Stat. Soc. Ser. B Methodol. 41, 368–374.
Rodriguez, E., Morris, C.S., Belz, J.E., 2006. A global assessment of the SRTM performance. Photogramm. Eng. Remote. Sens. 72, 249–260.
Rohrmüller, J., Kämpf, H., Geiß, E., Großmann, J., Grun, I., Mingram, J., Mrlina, J., Plessen, B., Stebich, M., Veress, C., Wendt, A., Nowaczyk, N., 2017. Reconnaissance study of an inferred Quaternary maar structure in the western part of the Bohemian Massif near Neualbenreuth, NE-Bavaria (Germany). Int. J. Earth Sci. 107, 1381–1405.
Runge, M.G., Bebbington, M.S., Cronin, S.J., Lindsay, J.M., Kenedi, C.L., Moufti, M.R.H., 2014. Vents to events: determining an eruption event record from volcanic vent structures for the Harrat Rahat, Saudi Arabia. Bull. Volcanol. 76, 804.
Runge, M.G., Bebbington, M.S., Cronin, S.J., Lindsay, J.M., Moufti, M.R., 2015. Sensitivity to volcanic field boundary. J. Appl. Volcanol. 4, 22.
Salzmann, U., 2000. Are modern savannas degraded forests? – a Holocene pollen record from the Sudanian vegetation zone of NE Nigeria. Veg. Hist. Archaeobotany 9, 1–15.
Sato, H., Aramaki, S., Kusakabe, M., Hirabayashi, J.-I., Sano, Y., Nojiri, Y., Tchoua, F., 1990. Geochemical difference of basalts between polygenetic and monogenetic volcanoes in the central part of the Cameroon volcanic line. Geochem. J. 24, 357–370.
Schmidt, C., Tchouankoue, J.P., Nkouamen Nemzoue, P.N., Ayaba, F., Nformidah-Ndah, S.S., Nformi Chifu, E., 2017a. New thermoluminescence age estimates for the Nyos maar eruption (Cameroon Volcanic Line). PLoS One 12, e0178545.
Schmidt, C., Schaarschmidt, M., Kolb, T., Büchel, G., Richter, D., Zöller, L., 2017b. Luminescence dating of late Pleistocene eruptions in the Eifel Volcanic Field, Germany. J. Quat. Sci. 32, 628–638.
Seib, N., Kley, J., Büchel, G., 2012. Identification of maars and similar volcanic landforms in the West Eifel Volcanic Field through image processing of DTM data: efficiency of different methods depending on preservation state. Int. J. Earth Sci. 102, 875–901.
Settle, M., 1979. The structure and emplacement of cinder cone fields. Am. J. Sci. 279, 1089–1107.
Smith, I.E.M., Cronin, S.J., 2021. Geochemical patterns of late Cenozoic intraplate basaltic volcanism in northern New Zealand and their relationship to the behaviour of the mantle. N. Z. J. Geol. Geophys. 64, 201–212.
Suh, C.E., Ayonghe, S.N., Sparks, R.S.J., Annen, C., Fitton, J.G., Nana, R., Luckman, A., 2003. The 1999 and 2000 eruptions of Mount Cameroon: eruption behaviour and petrochemistry of lava. Bull. Volcanol. 65, 267–281.
Tamen, J., Nkoumbou, C., Mouafo, L., Reusser, E., Tchoua, F.M., 2007. Petrology and geochemistry of monogenetic volcanoes of the Barombi Koto volcanic field (Kumba graben, Cameroon volcanic line): Implications for mantle source characteristics. Compt. Rendus Geosci. 339, 799–809.
Tchaptchet, D.T., Wambo, N.A.S., Kouamo, N.A.K., Tchouankoué, J.-P., Cucciniello, C., 2017. Geology, mineralogy and geochemistry of the Kekem dyke swarm (Western Cameroon): insights into Paleozoic–Mesozoic magmatism and geodynamic implications. Compt. Rendus Geosci. 349, 175–185.
Tedla, G.E., Meijde, M.V.D., Nyblade, A.A., Meer, F.D.V.D., 2011. A crustal thickness map of Africa derived from a global gravity field model using Euler deconvolution. Geophys. J. Int. 187, 1–9.
Temdjim, R., Njilah, I.K., Kamgang, P., Nkoumbou, C., 2004. Donnees nouvelles sur les laves felsiques de Ngaoundere (Adamaoua, ligne du Cameroun): chronologie K-Ar et petrologie. Afr. J. Sci. Technol. 5.
Temdjim, R., Njombie Wagsong, M.P., Nzakou Tsepeng, A.J., Foley, S., 2020. Variation in mantle lithology and composition beneath the Ngao Bilta volcano, Adamawa Massif, Cameroon volcanic line, West-central Africa. Geosci. Front. 11, 665–677.
Tiabou, A.F., Temdjim, R., Wandji, P., Bardintzeff, J.-M., Che, V.B., Bate Tibang, E.E., Ngwa, C.N., Mebara, F.X.O., 2019. Baossi–Warack monogenetic volcanoes, Adamawa Plateau, Cameroon: petrography, mineralogy and geochemistry. Acta Geochim. 38, 40–67.
Valente, F., Cruz, J.V., Pimentel, A., Coutinho, R., Andrade, C., Nemésio, J., Cordeiro, S., 2022. Evaluating the impact of explosive volcanic eruptions on a groundwater-fed water supply system: an exploratory study in Ponta Delgada, São Miguel (Azores, Portugal). Water 14, 1022.
Valentine, G.A., Connor, C.B., 2015. Basaltic volcanic fields. In: Sigurdsson, H. (Ed.), The Encyclopedia of Volcanoes, Amsterdam, pp. 423–439.
Valentine, G.A., Cortés, J.A., Widom, E., Smith, E.I., Rasoazanamparany, C., Johnsen, R., Briner, J.P., Harp, A.G., Turrin, B., 2017. Lunar Crater volcanic field (Reveille and Pancake Ranges, Basin and Range Province, Nevada, USA). Geosphere 13, 391–438.
Vörös, F., van Wyk de Vries, B., Karátson, D., Székely, B., 2021. DTM-Based Morphometric Analysis of Scoria Cones of the Chaîne des Puys (France)—the Classic and a New Approach. Remote Sens. 13, 1983.
Wandji, P., Wotchoko, P., Bardintzeff, J.M., Bellon, H., 2010. Late Tertiary and Quaternary alkaline volcanism in the western Noun Plain (Cameroon Volcanic Line): New K-Ar ages, petrology and isotope data. Geochem. Mineral. Petrol. 48, 67–94.
Watts, P., Waythomas, C.F., 2003. Theoretical analysis of tsunami generation by pyroclastic flows. J. Geophys. Res. 108.
Wembenyui, E.W., Collerson, K.D., Zhao, J.-X., 2020. Evolution of Mount Cameroon volcanism: Geochemistry, mineral chemistry and radiogenic isotopes (Pb, Sr, Nd). Geosci. Front. 11, 2157–2168.
Wilson, G., Wilson, T.M., Deligne, N.I., Cole, J.W., 2014. Volcanic hazard impacts to critical infrastructure: a review. J. Volcanol. Geotherm. Res. 286, 148–182.
Wood, C.A., 1980. Morphometric analysis of cinder cone degradation. J. Volcanol. Geotherm. Res. 8, 137–160.
Wotchoko, P., Wandji, P., Bardintzeff, J.-M., Bellon, H., 2005. Données pétrologiques et géochronologiques nouvelles sur le volcanisme alcalin néogène à récent de la rive ouest du Noun (plaine du Noun, Ligne du Cameroun). Rev. Bulgar. Geol. Soc. 66, 97–105.
Yamgouot, F.N., Déruelle, B., Gbambié Mbowou, I.B., Ngounouno, I., Demaiffe, D., 2016. Geochemistry of the volcanic rocks from Bioko Island ("Cameroon Hot Line"): evidence for plume-lithosphere interaction. Geosci. Front. 7, 743–757.
Yokoyama, T., Aka, F.T., Kusakabe, M., Nakamura, E., 2007. Plume–lithosphere interaction beneath Mt. Cameroon volcano, West Africa: Constraints from ^{238}U–^{230}Th–^{226}Ra and Sr–Nd–Pb isotope systematics. Geochim. Cosmochim. Acta 71, 1835–1854.
Zarazúa-Carbajal, M.C., De la Cruz-Reyna, S., 2020. Morpho-chronology of monogenetic scoria cones from their level contour curves. Applications to the Chichinautzin monogenetic field, Central Mexico. J. Volcanol. Geotherm. Res. 407, 107093.
Zogning, A., Giresse, P., Maley, J., Gadel, F., 1997. The late holocene palaeoenvironment in the Lake Njupi area, West Cameroon: implications regarding the history of Lake Nyos. J. Afr. Earth Sci. 24, 285–300.